

# The SAURON project – IX. A kinematic classification for early-type galaxies

Eric Emsellem,<sup>1★</sup> Michele Cappellari,<sup>2,3</sup> Davor Krajnović,<sup>3</sup> Glenn van de Ven,<sup>2,4,5★</sup>  
 R. Bacon,<sup>1</sup> M. Bureau,<sup>3</sup> Roger L. Davies,<sup>3</sup> P. T. de Zeeuw,<sup>2</sup> Jesús Falcón-Barroso,<sup>2,6</sup>  
 Harald Kuntschner,<sup>7</sup> Richard McDermid,<sup>2</sup> Reynier F. Peletier<sup>8</sup> and Marc Sarzi<sup>9</sup>

<sup>1</sup> *Université de Lyon, France; université Lyon 1, F-69007; CRAL, Observatoire de Lyon, F-69230 Saint Genis Laval; CNRS, UMR 5574; ENS de Lyon, France*

<sup>2</sup> *Sterrewacht Leiden, Leiden University, Niels Bohrweg 2, 2333 CA Leiden, the Netherlands*

<sup>3</sup> *Sub-Department of Astrophysics, University of Oxford, Denys Wilkinson Building, Keble Road, Oxford OX1 3RH*

<sup>4</sup> *Department of Astrophysical Sciences, Peyton Hall, Princeton, NJ 08544, USA*

<sup>5</sup> *Institute for Advanced Study, Einstein Drive, Princeton, NJ 08540, USA*

<sup>6</sup> *European Space and Technology Centre (ESTEC), Keplerlaan 1, Postbus 299, 2200 AG Noordwijk, the Netherlands*

<sup>7</sup> *Space Telescope European Coordinating Facility, European Southern Observatory, Karl-Schwarzschild-Str 2, 85748 Garching, Germany*

<sup>8</sup> *Kapteyn Astronomical Institute, Postbus 800, 9700 AV Groningen, the Netherlands*

<sup>9</sup> *Centre for Astrophysics Research, University of Hertfordshire, Hatfield, Herts AL10 9AB*

Accepted 2007 March 19. Received 2007 March 12; in original form 2006 August 4

## ABSTRACT

Two-dimensional stellar kinematics of 48 representative elliptical (E) and lenticular (S0) galaxies obtained with the SAURON integral-field spectrograph reveal that early-type galaxies appear in two broad flavours, depending on whether they exhibit clear large-scale rotation or not. We define a new parameter  $\lambda_R \equiv \langle R |V| \rangle / \langle R \sqrt{V^2 + \sigma^2} \rangle$ , which involves luminosity-weighted averages over the full two-dimensional kinematic field as a proxy to quantify the observed projected stellar angular momentum per unit mass. We use it as a basis for a new kinematic classification: early-type galaxies are separated into slow and fast rotators, depending on whether they have  $\lambda_R$  values within their effective radius  $R_e$  below or above 0.1, respectively. Slow and fast rotators are shown to be physically distinct classes of galaxies, a result which cannot simply be the consequence of a biased viewing angle. Fast rotators tend to be relatively low-luminosity galaxies with  $M_B \gtrsim -20.5$ . Slow rotators tend to be brighter and more massive galaxies, but are still spread over a wide range of absolute magnitude. Three slow rotators of our sample, among the most massive ones, are consistent with zero rotation. Remarkably, all other slow rotators (besides the atypical case of NGC 4550) contain a large kpc-scale kinematically decoupled core (KDC). All fast rotators (except one galaxy with well-known irregular shells) show well-aligned photometric and kinematic axes, and small velocity twists, in contrast with most slow rotators which exhibit significant misalignments and velocity twists. These results are supported by a supplement of 18 additional early-type galaxies observed with SAURON. In a companion paper (Paper X), we also show that fast and slow rotators are distinct classes in terms of their orbital distribution. We suggest that gas is a key ingredient in the formation and evolution of fast rotators, and that the slowest rotators are the extreme evolutionary end point reached deep in gravitational potential wells where dissipationless mergers had a major role in the evolution, and for which most of the baryonic angular momentum was expelled outwards. Detailed numerical simulations in a cosmological context are required to understand how to form large-scale KDCs within slow rotators, and

★E-mail: emsellem@obs.univ-lyon1.fr

more generally to explain the distribution of  $\lambda_R$  values within early-type galaxies and the distinction between fast and slow rotators.

**Key words:** galaxies: elliptical and lenticular, cD – galaxies: evolution – galaxies: formation – galaxies: kinematics and dynamics – galaxies: structure.

## 1 INTRODUCTION

The origin of the classification fork for galaxies can be found in an early paper by Jeans (1929), with the lenticulars (S0s) as a class being introduced by Hubble (1936) to account for the important population of flattened objects in nearby clusters (Spitzer & Baade 1951). In a recent debate on galaxy classification, Sandage (2004) mentioned that the simplest definition of a S0 galaxy remains ‘a disc galaxy more flattened than an E6 elliptical but with no trace of spiral arms or recent star formation’. Elliptical (E) and S0 galaxies are usually gathered into the so-called early-type category, and are recognized to share a number of global properties (de Vaucouleurs et al. 1991) such as their relatively low dust and interstellar gas content and their overall red colours. The Hubble sequence is, however, seen as a continuous one between Es and spirals, with the S0s occupying the transition region with typical bulge to disc ratios of  $\sim 0.6$ . S0s are thus considered disc-dominated galaxies, while Es are spheroid dominated.

Such contrived galaxy types may be misleading, most evidently because ‘the sequence E0–E6 is one of apparent flattening’ (Kormendy & Bender 1996, hereafter KB96). A modern classification scheme should go beyond a purely descriptive tool, and should therefore encompass part of our knowledge of the physical properties of these objects.<sup>1</sup> This was advocated by KB96 who wished to update the Hubble sequence by sorting Es in terms of the importance of rotation for their stellar dynamical state. They used the disciness or boxiness of the isophotes to quantify anisotropy and to define refined types: E(d) galaxies (for discy Es) making the link between S0s and E(b) galaxies (for boxy Es). The disciness (or boxiness) was then provided by a measure of the now classical normalized  $a_4/a$  term (see Bender, Doebereiner & Moellenhoff 1988, for details): positive and negative  $a_4/a$  terms correspond to discy and boxy deviations from ellipses, respectively.

This extension of the Hubble types has the merit of upgrading our view of Es and S0s via some easily accessible observable parameter, and it follows the philosophy that a mature classification scheme should include some physics into the sorting criteria. It does, however, use a photometric indicator as an attempt to quantify the dynamical state of the galaxy, which may be unreliable. More importantly, it conserves the dichotomy between S0s and Es, relying on the old (and ambiguous) definition of a S0.

We have recently conducted a survey of 72 early-type (E, S0, Sa) galaxies using the integral-field spectrograph SAURON mounted on the William Herschel Telescope in La Palma (Bacon et al. 2001, hereafter Paper I; de Zeeuw et al. 2002, hereafter Paper II). This allowed us to map the stellar and gas kinematics as well as a number of stellar absorption line indices up to about one effective radius  $R_e$  for most of the galaxies in the sample. The two-dimensional stellar kinematics for the 48 E and S0 galaxies (Emsellem et al. 2004, hereafter Paper III) show a wide variety of features such

as kinematically decoupled or counter-rotating cores, central discs and velocity twists. More importantly, there seem to be two broad classes of observed stellar velocity fields, with galaxies in one class exhibiting a clear large-scale rotation pattern and those in the other showing no significant rotation (Fig. 1). The existence of these two classes must be linked to the formation and evolution of early-type galaxies, and is in any case a key to understand their dynamical state (see also Cappellari et al. 2006, hereafter Paper IV).

Using the unique data set obtained in the course of the SAURON project, we here revisit the early-type galaxy classification issues mentioned above, using the available full two-dimensional kinematic information. A companion paper (Cappellari et al. 2007, hereafter Paper X) examines in more detail the orbital anisotropy of E and S0 galaxies using the same data set. After a brief presentation of the data set and methods (Section 2), we define a new parameter as a proxy to robustly quantify the angular momentum of galaxies (Section 3). In Section 4, we examine how this parameter relates to both more standard photometric classification schemes including de Vaucouleurs morphological classification of Es and S0s (de Vaucouleurs et al. 1991) or the revision of the Hubble sequence by KB96, and kinematic properties of early-type galaxies (Section 4.4). We then briefly discuss the implications of our results on the potential scenarios for the formation and evolution of these galaxies (Section 5), and conclude in Section 6.

## 2 DATA AND METHODS

### 2.1 The SAURON sample of E and S0s

The SAURON sample has been designed as a *representative* sample of 72 nearby ( $cz < 3000 \text{ km s}^{-1}$ ) early-type galaxies in the plane of ellipticity  $\epsilon$  versus absolute  $B$ -band magnitude  $M_B$ . We restricted the sample to 24 objects for each of the E, S0 and Sa classes, with 12 ‘cluster’ and 12 ‘field’ targets in each group. Although this sample is itself not a complete one, it has been drawn in a homogeneous way from a complete sample of more than 300 galaxies (see Paper II for more details about the full SAURON sample). We will therefore solely focus on the SAURON E+S0 sample (which thus contains 48 galaxies) for conducting our analysis in Sections 2 to 4. An additional set of 18 E+S0 galaxies has been independently observed with a similar SAURON setup in the course of various other projects. These objects will be treated as ‘specials’, most having features which motivated a specific observation, and will be only briefly mentioned in Section 5 to confront the obtained results.

### 2.2 Photometry

Ground-based photometric MDM Observatory data (Falcón-Barroso et al., in preparation) were obtained for all galaxies of the SAURON sample. We also made use of additional *Hubble Space Telescope* Wide Field Planetary Camera 2 (*HST/WPFC2*) data which are available for 42 galaxies out of the 48 E/S0. SAURON-reconstructed images were used as well to directly derive a global

<sup>1</sup> For the written transcript of a debate on this issue, see Sandage (2004) and the panel discussion in the same proceedings.

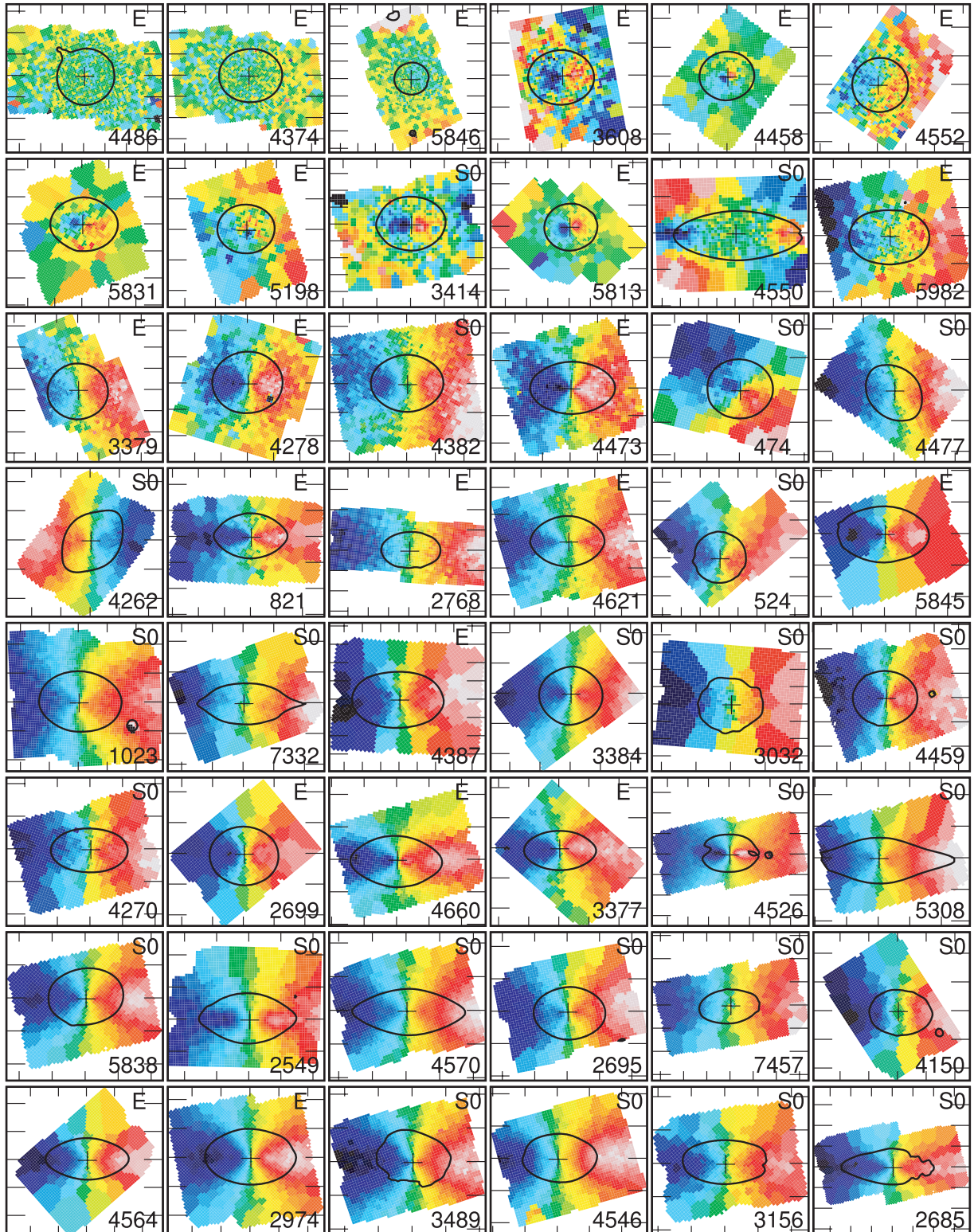


**Figure 1.** SAURON stellar velocity fields for our 48 E and S0 galaxies (see Paper III), the global outer photometric axis being horizontal. Colour cuts were tuned for each individual galaxy as to properly emphasize the observed velocity structures. A representative isophote is overplotted in each thumbnail as a black solid line, and the centre is marked with a cross. Galaxies are ordered by increasing value of  $\lambda_{R_e}$  (from left to right-hand side, top to bottom; see Section 3). Slow rotators are galaxies on the first two rows. NGC numbers and Hubble types are provided in the lower-right and upper-right corners of each panel, respectively. Tick marks correspond to 10 arcsec.

ellipticity  $\epsilon$  via moments of the surface brightness images as

$$\epsilon \equiv 1 - \sqrt{\frac{\langle y^2 \rangle}{\langle x^2 \rangle}}, \quad (1)$$

where  $x$  and  $y$  are the sky coordinates along the photometric major and minor axes, respectively (see Paper X for details). The brackets  $\langle \rangle$  correspond to a flux-weighted sky average as in

$$\langle G \rangle = \frac{\sum_{i=1}^{N_p} F_i G_i}{\sum_{i=1}^{N_p} F_i}, \quad (2)$$

where the sums extend over a pre-defined region on the sky, with  $N_p$  the number of pixels and  $F_i$  the flux value within the  $i$ th pixel. In the following sections, we denote  $\epsilon$  and  $\epsilon_{1/2}$  as the global ellipticity computed from the SAURON data within  $1R_e$  and  $R_e/2$  or restricted to the equivalent effective aperture of the SAURON field of view, whichever is smaller. These will be used in Section 3, where we examine kinematic quantities derived from SAURON data as a function of the flux-weighted global ellipticity.

We also obtained radial profiles for the ellipticity and  $a_4/a$  (with  $a$  the ellipse semimajor-axis) parameters from the MDM and *HST*/WPC2 photometric data sets using the `GALPHOT` package (Franx, Illingworth & Heckman 1989). We then derived  $\epsilon_e$  and  $(a_4/a)_e$ , the mean ellipticity and  $a_4/a$  values within  $1R_e$ , by taking the flux-weighted average of the `GALPHOT` profiles taking into account the corresponding sky area. More specifically, the mean  $G_e$  of a quantity  $G(R)$  within  $1R_e$  derived from its radial profile, where  $R$  is the semimajor-axis radius, is defined as (see e.g. Ryden et al. 1999)

$$G_e = \frac{\int_0^{R_e} q(R)F(R)G(R)R dR}{\int_0^{R_e} q(R)F(R)R dR}, \quad (3)$$

where  $q(R)$  and  $\Sigma(R)$  are, respectively, the best-fitting ellipse axis ratio and surface brightness profiles. Using the sampled radial profiles, we approximate this with

$$G_e \sim \frac{\sum_{k=1}^N q(R_k)F(R_k)G(R_k)(R_{\text{out},k}^2 - R_{\text{in},k}^2)}{\sum_{k=1}^N q(R_k)F(R_k)(R_{\text{out},k}^2 - R_{\text{in},k}^2)}, \quad (4)$$

where  $R_{\text{in},k}$  and  $R_{\text{out},k}$  correspond to the inner and outer radii of the  $k$ th annulus. The values for  $\epsilon$ ,  $\epsilon_e$  and  $(a_4/a)_e$  are provided in Table 1. Observed differences between  $\epsilon$  and  $\epsilon_e$  values are almost always smaller than 0.1, and due to their respective luminosity weighting.  $\epsilon$  is measured directly from the SAURON data, and will therefore be confronted with other quantities measured from the same data set, while  $\epsilon_e$  being derived from one-dimensional radial profiles can serve in comparison with previous works. For both  $\epsilon_e$  and  $(a_4/a)_e$ , the overall agreement between our values and published ones (Bender, Saglia & Gerhard 1994) is excellent (see Paper X for a detailed comparison).

Results from fitting Sersic and Sersic-core laws (Trujillo et al. 2004; Ferrarese et al. 2006) to the radial luminosity profiles will be presented in detail in a subsequent paper of this series (Falc3n-Barroso et al., in preparation). In the present paper, we will only mention trends (Section 4.3), considering the Sersic index  $n$  (where  $n = 1$  corresponds to an exponential luminosity profile, and  $n = 4$  to a de Vaucouleurs  $R^{1/4}$  law), as well as the classification of the central photometric profiles with either shallow or steep inner cusps, labelled, respectively, as ‘cores’ and ‘power laws’ (Faber et al. 1997; Ravindranath et al. 2001; Rest et al. 2001; Lauer et al. 2005).

### 2.3 The SAURON data

SAURON is an integral-field spectrograph built at Lyon Observatory and mounted since 1999 February at the Cassegrain focus of the William Herschel Telescope. It is based on the TIGER concept (Bacon et al. 1995), using a microlens array to sample the field of view. Details of the instrument can be found in Papers I and II. All 48 E and S0 galaxies were observed with the low-resolution mode of SAURON which covers a field of view of about  $33 \times 41$  arcsec<sup>2</sup> with  $0.94 \times 0.94$  arcsec<sup>2</sup> per square lens. Mosaicking was used to cover up to a radius of  $1R_e$ . Only for the two galaxies with the largest  $R_e$  (NGC 4486 and 5846) do we reach a radius of  $\sim R_e/3$  only.

All data reduction was performed using the dedicated `XSAURON` software wrapped in a scripted pipeline (Paper II). For each target, individual datacubes were merged and analysed as described in Paper III, ensuring a minimum signal-to-noise ratio of 60 per pixel using the binning scheme developed by Cappellari & Copin (2003). The SAURON stellar kinematics were derived using a penalized pixel fitting routine (Cappellari & Emsellem 2004), which provides parametric estimates of the line-of-sight velocity distribution (hereafter LOSVD) for each spaxel. In Paper III, we have presented the corresponding maps, which include the mean velocity  $V$ , the velocity dispersion  $\sigma$  and the Gauss–Hermite moments  $h_3$  and  $h_4$ , for the 48 E and S0 SAURON galaxies.

As mentioned in Paper III, these quantities were measured fitting all  $V$ ,  $\sigma$ ,  $h_3$  and  $h_4$  simultaneously: this ensures an optimal representation of the corresponding LOSVD. In the present paper, we focus on the first two true velocity moments,  $\mu_1$  and  $\mu_2$ , which are sometimes estimated by using the Gauss–Hermite expansion of the LOSVD (van der Marel & Franx 1993). As emphasized in Paper IV, the second-order velocity moment is very sensitive to the details of the high-velocity wings, which can rarely be accurately measured. We therefore decided to rely on a simpler but more robust single Gaussian fit (excluding higher-order velocity moments), and used the Gaussian mean  $V$  and standard deviation  $\sigma$  to approximate the first and second velocity moments.

### 2.4 Kinemetry

Following Krajnović et al. (2006), who recently advocated the use of a method generalizing the isophotal-shape tools (Lauer 1985; Bender & Moellenhoff 1987; Jedrzejewski 1987), we employ kinemetry as a quantitative approach to analyse the SAURON stellar kinematic maps. Applying kinemetry on a velocity map provides radial profiles for the kinematic position angle  $\text{PA}_{\text{kin}}$ , axis ratio  $q_{\text{kin}}$  and Fourier kinemetry terms, the dominant term  $k_1$  representing the velocity amplitude. We define a kinematic component to have constant or slowly varying  $\text{PA}_{\text{kin}}$  and  $q_{\text{kin}}$  radial profiles (taking into account the derived error bars). We then identify two separate components when we observe an abrupt change either with  $\Delta q_k > 0.1$ , or  $\Delta \text{PA}_{\text{kin}} > 10^\circ$ , or with a double-hump in  $k_1$  with a local minimum in between. The transition between the two radial ranges is often emphasized by a peak in the higher-order  $k_5$  Fourier term, which thus serves as an additional signature for such a change (Krajnović et al. 2006). Velocity maps which exhibit the presence of at least two stellar velocity components are tagged as *Multiple Component* (MC), as opposed to *Single Component* (SC).

We use a number of terms to represent some basic properties of the individual kinematic components via quantitative criteria, following the definitions provided in Krajnović et al. (2006):

**Table 1.** Characteristics of the E and S0 galaxies in the representative SAURON sample. All galaxies with  $\lambda_{R_e} > 0.1$  are classified as fast rotators.

Galaxy (NGC)	Type	$T$	$(m - M)$ (mag)	$M_B$ (mag)	$R_e$ (arcsec)	$\sigma'_e$ ( $\text{km s}^{-1}$ )	$\epsilon_{1/2}$	$\epsilon$	$\epsilon_e$	$(a_4/a)_e$	$V/\sigma$	$\lambda_{R_e}$	Group	Rotator
(1)	(2)	(3)	(4)	(5)	(6)	(7)	(8)	(9)	(10)	(11)	(12)	(13)	(14)	(15)
474	S0 <sup>0</sup> (s)	−2.0	32.56	−20.42	29	150	0.11	0.11	0.13	−0.14	0.21	0.200	MC	F
524	S0 <sup>+</sup> (rs)	−1.2	31.84	−21.40	51	235	0.05	0.05	0.04	−0.16	0.29	0.278	SC	F
821	E6?	−4.8	31.85	−20.44	39	189	0.40	0.40	0.35	1.43	0.26	0.258	SC	F
1023	SB0 <sup>−</sup> (rs)	−2.7	30.23	−20.42	48	182	0.33	0.33	0.36	0.54	0.35	0.385	SC	F
2549	S0 <sup>0</sup> (r) sp	−2.0	30.44	−19.36	20	145	0.47	0.49	0.49	2.86	0.56	0.539	MC	F
2685	(R)SB0 <sup>+</sup> pec	−1.1	31.15	−19.05	20	96	0.56	0.62	0.59	2.93	0.88	0.716	SC	F
2695	SAB0 <sup>0</sup> (s)	−2.1	32.49	−19.38	21	188	0.27	0.29	0.21	0.36	0.54	0.561	MC	F
2699	E:	−5.0	32.09	−18.85	14	124	0.16	0.15	0.19	1.04	0.43	0.450	MC	F
2768	E6:	−4.3	31.69	−21.15	71	216	0.38	0.38	0.46	0.12	0.24	0.268	SC	F
2974	E4	−4.7	31.60	−20.32	24	233	0.38	0.37	0.37	0.64	0.70	0.602	SC	F
3032	SAB0 <sup>0</sup> (r)	−1.8	31.65	−18.77	17	90	0.15	0.11	0.17	0.44	0.27	0.416	CLV	F
3156	S0:	−2.4	31.69	−18.08	25	65	0.49	0.47	0.47	−0.04	0.88	0.713	SC	F
3377	E5-6	−4.8	30.19	−19.24	38	138	0.46	0.46	0.50	0.94	0.49	0.475	SC	F
3379	E1	−4.8	30.06	−20.16	42	201	0.08	0.08	0.11	0.16	0.14	0.145	SC	F
3384	SB0 <sup>−</sup> (s):	−2.7	30.27	−19.56	27	145	0.20	0.20	0.20	1.13	0.44	0.414	MC	F
3414	S0 pec	−2.1	31.95	−19.78	33	205	0.21	0.21	0.23	1.80	0.09	0.062	KDC	S
3489	SAB0 <sup>+</sup> (rs)	−1.3	30.35	−19.32	19	98	0.28	0.29	0.29	−0.61	0.67	0.602	MC	F
3608	E2	−4.8	31.74	−19.54	41	178	0.18	0.18	0.20	−0.21	0.05	0.038	KDC	S
4150	S0 <sup>0</sup> (r)?	−2.1	30.64	−18.48	15	77	0.25	0.30	0.28	−0.32	0.58	0.584	CLV	F
4262	SB0 <sup>−</sup> (s)	−2.7	31.23	−18.88	10	172	0.08	0.22	0.11	1.28	0.24	0.245	MC	F
4270	S0	−1.9	32.83	−18.28	18	122	0.41	0.50	0.44	−0.64	0.40	0.446	MC	F
4278	E1-2	−4.8	30.97	−19.93	32	231	0.12	0.12	0.13	−0.15	0.18	0.149	MC	F
4374	E1	−4.2	31.27	−21.23	71	278	0.15	0.15	0.13	−0.40	0.03	0.023	SC	S
4382	S0 <sup>+</sup> (s) pec!	−1.3	31.27	−21.28	67	196	0.19	0.19	0.22	0.59	0.16	0.155	CLV	F
4387	E	−4.8	31.59	−18.34	17	98	0.35	0.40	0.32	−0.76	0.39	0.408	SC	F
4458	E0-1	−4.8	31.12	−18.42	27	85	0.12	0.12	0.14	0.41	0.12	0.046	KDC	S
4459	S0 <sup>+</sup> (r)	−1.4	30.98	−19.99	38	168	0.18	0.17	0.17	0.22	0.45	0.436	MC	F
4473	E5	−4.7	30.92	−20.26	27	192	0.39	0.41	0.43	1.03	0.22	0.195	MC	F
4477	SB0(s):?	−1.9	31.07	−19.96	47	162	0.24	0.24	0.23	2.04	0.21	0.215	SC	F
4486	E0-1 <sup>+</sup> pec	−4.3	30.97	−21.79	105	298	0.04	0.04	0.07	−0.07	0.02	0.019	SC	S
4526	SAB0 <sup>0</sup> (s):!	−1.9	31.08	−20.68	40	222	0.36	0.37	0.41	−1.92	0.54	0.476	MC	F
4546	SB0 <sup>−</sup> (s):	−2.7	30.69	−19.98	22	194	0.39	0.45	0.36	0.69	0.60	0.604	MC	F
4550	SB0 <sup>0</sup> :sp	−2.0	30.94	−18.83	14	110	0.58	0.61	0.62	2.36	0.10	0.091	MC	S
4552	E0-1	−4.6	30.86	−20.58	32	252	0.04	0.04	0.06	0.00	0.05	0.049	KDC	S
4564	E	−4.8	30.82	−19.39	21	155	0.47	0.52	0.43	1.33	0.58	0.586	SC	F
4570	S0 sp	−2.0	31.23	−19.54	14	173	0.41	0.60	0.44	1.90	0.53	0.561	MC	F
4621	E5	−4.8	31.25	−20.64	46	211	0.34	0.34	0.35	1.66	0.25	0.268	KDC	F
4660	E	−4.7	30.48	−19.22	11	185	0.33	0.44	0.41	0.66	0.49	0.472	MC	F
5198	E1-2:	−4.7	33.06	−20.38	25	179	0.14	0.12	0.14	−0.17	0.07	0.060	KDC	S
5308	S0 <sup>−</sup> sp	−2.0	32.65	−20.27	10	208	0.32	0.60	0.53	4.74	0.45	0.483	MC	F
5813	E1-2	−4.8	32.38	−20.99	52	230	0.15	0.15	0.17	−0.03	0.14	0.063	KDC	S
5831	E3	−4.8	32.11	−19.73	35	151	0.15	0.15	0.20	0.46	0.08	0.049	KDC	S
5838	S0 <sup>−</sup>	−2.7	32.37	−19.87	23	240	0.27	0.34	0.28	0.34	0.51	0.518	MC	F
5845	E:	−4.8	32.01	−18.58	4	239	0.35	0.35	0.31	0.63	0.36	0.357	MC	F
5846	E0-1	−4.7	31.92	−21.24	81	238	0.07	0.07	0.07	−0.38	0.03	0.024	SC	S
5982	E3	−4.8	33.15	−21.46	27	229	0.30	0.30	0.28	−0.92	0.08	0.093	KDC	S
7332	S0 pec sp	−2.0	31.40	−19.93	11	125	0.40	0.42	0.39	1.35	0.32	0.390	KDC	F
7457	S0 <sup>−</sup> (rs)?	−2.6	30.55	−18.81	65	78	0.44	0.44	0.43	0.20	0.62	0.570	CLV	F

Notes: (1) Galaxy identifier (NGC number). (2) Hubble type (NED). (3) Numerical morphological type (LEDA; Paturel et al. 2003). (4) Galaxy distance modulus from Tonry et al. (2001), Tully (1988) (corrected by subtracting 0.06 mag; see Mei et al. 2005), or from the LEDA data base assuming a Hubble flow with  $H = 75 \text{ km s}^{-1} \text{ Mpc}^{-1}$ . (5) Absolute  $B$  magnitude (Paper II). (6) Effective radius in arcsec. (7) Velocity dispersion derived using the luminosity-weighted spectrum within  $R_e$  or within the SAURON field, whichever is smaller. (8) and (9) Global ellipticity within  $R_e/2$  and  $R_e$  (from SAURON), or within the SAURON field, whichever is smaller. (10) Mean ellipticity within  $1R_e$ , derived from the GALPHOT radial profile. (11) Mean isophote shape parameter  $a_4/a$  (in per cent) within  $1R_e$ . (12) and (13)  $V/\sigma$  (see Paper X) and  $\lambda_R$  within  $1R_e$ . (14) Kinemetry group (see Section 2.4). (15) Rotator class: F = fast, S = slow.



(i) *Low-level velocity (LV)*: defined when the maximum velocity amplitude  $k_1$  is lower than  $15 \text{ km s}^{-1}$ . Note that when the velocity amplitude is constant over the field,  $\text{PA}_{\text{kin}}$  and  $q_{\text{kin}}$  are ill defined. When the central kinematical component is LV, we label the galaxy as a central low-level velocity (CLV) system.

(ii) *Kinematic misalignment (KM)*: defined when the absolute difference between the photometric and kinematic position angles ( $\text{PA}_{\text{phot}}$  and  $\text{PA}_{\text{kin}}$ ) is larger than  $10^\circ$ .

(iii) *Kinematic twist (KT)*: defined by a smooth variation of the kinematic position angle  $\text{PA}_{\text{kin}}$  with an amplitude of at least  $10^\circ$  within the extent of the kinematic component.

A *kinematically decoupled component (KDC)* is defined as a MC having either an abrupt change in  $\text{PA}_{\text{kin}}$ , with a difference larger than  $20^\circ$  between two adjacent components, or an outer LV kinematic component (which prevents that component to have a robust  $\text{PA}_{\text{kin}}$  measurement). This definition roughly corresponds to the more standard appellation of KDC used in the past (Bender 1988), although the two-dimensional coverage provided by integral-field spectrographs allows a more sensitive detection procedure. These kinematic components will be examined in Section 4.4.

### 3 QUANTIFYING THE ANGULAR MOMENTUM

The velocity fields presented in Paper III revealed a wealth of structures such as decoupled cores, velocity twists, misalignments, cylindrical or disc-like rotation (see also Section 4.4). It is difficult to disentangle the relative contributions of a true variation in the internal dynamical state and the effect of projection. The first examination of the stellar velocity maps for the 48 SAURON E/S0 galaxies (Fig. 1, where velocity cuts have been adjusted as to properly emphasize the observed velocity structures) suggests that early-type galaxies come in two broad flavours: one which exhibits a clear large-scale and rather regular rotation pattern, and another which shows perturbed velocity structures (e.g. strong velocity twists) or central KDCs with little rotation in the outer regions. One way to constrain the internal dynamics for a specific galaxy is to build a detailed model using all available observables. This was successfully achieved in Paper IV on a subsample of 24 galaxies, for which accurate distances and high spatial resolution photometry are available, and where no strong signature of non-axisymmetry is observed. From these models, a considerable amount of detail on the orbital structure was derived (see also Paper X). We, however, also need a simple measurable parameter which quantifies the (apparent) *global* dynamical state of a galaxy, and which is applicable to all galaxies in our representative sample of Es and S0s: this is the purpose of this section.

#### 3.1 From $V/\sigma$ to $\lambda_R$ : a new kinematic parameter

The relation of  $V/\sigma$  versus mean ellipticity  $\epsilon$  (hereafter the anisotropy diagram) was often used in the past to confront the apparent flattening with the observed amount of rotation (Illingworth 1977; Binney 1978; Davies et al. 1983). In the now classical treatment of the anisotropy diagram, the maximum observed rotational velocity  $V_{\text{max}}$  and the central dispersion  $\sigma_0$  are generally used as surrogates for the mass-weighted mean of the square rotation speed and the random velocity. This was mostly constrained by the fact that stellar kinematics were available along at most a few axes via long-slit spectroscopy. Binney (2005) has recently revisited this diagram to design a more robust diagnostic of the velocity anisotropy in galaxies using two-dimensional kinematic information. Start-

ing from the Tensor Virial Theorem, Binney reformulated the ratio of ordered versus random motions in terms of integrated quantities observable with integral-field spectrographs such as SAURON, namely  $\langle V^2 \rangle$  and  $\langle \sigma^2 \rangle$ , where  $V$  and  $\sigma$ , respectively, denote the observed stellar velocity and velocity dispersion, and the brackets correspond to a sky averaging weighted by the surface brightness (see equation 2).

The SAURON data provide us with a unique opportunity to derive for the first time a robust measurement of  $V/\sigma$  for a sample of local early-type galaxies. We have therefore derived  $\langle V^2 \rangle$  and  $\langle \sigma^2 \rangle$  up to  $\sim 1R_e$ , the resulting  $V/\sigma$  values for the 48 SAURON E and S0 galaxies being given in Table 1. S0s and Es tend to have on average relatively high and low  $V/\sigma$ , respectively. A very significant overlap of the two types still exists, S0s reaching values of  $V/\sigma$  as low as 0.1, and Es as high as 0.7: as expected, the Hubble type can obviously not serve as a proxy for the galaxy kinematics (see the distribution of Hubble types in Fig. 1).

The availability of two-dimensional stellar kinematics makes  $V/\sigma$  a useful tool to examine the dynamical status of early-type galaxies (see Paper X). It fails, however, to provide us with a way to differentiate mean stellar velocity structures as different as those of NGC 3379 and 5813 (see Fig. 1). These two galaxies both have  $V/\sigma \sim 0.14$ , and ellipticities  $\epsilon$  in the same range (0.08 and 0.15, respectively), but their stellar velocity fields are qualitatively and quantitatively very different: NGC 3379 displays a regular and large-scale rotation pattern with a maximum amplitude of about  $60 \text{ km s}^{-1}$ , whereas NGC 5813 exhibits clear central KDC with a peak velocity amplitude of  $\sim 85 \text{ km s}^{-1}$  and a mean stellar velocity consistent with zero outside a radius of  $\sim 12 \text{ arcsec}$ . The derivation of  $V/\sigma$  includes a luminosity weighting that amplifies the presence of the KDC in NGC 5813. As a consequence, NGC 3379 with its global rotation and NGC 5813 with its spatially confined non-zero velocities end up with a similar  $V/\sigma$ .

We therefore need to design a new practical way to quantify the global velocity structure of galaxies using the two-dimensional spatial information provided by integral-field units. The ideal tool would be a physical parameter which captures the spatial information included in the kinematic maps. Since we wish to assess the level of rotation in galaxies, this parameter should follow the nature of the classic  $V/\sigma$ : ordered versus random motion. A measure of the averaged angular momentum  $L = \langle \mathbf{R} \wedge \mathbf{V} \rangle$  could play the role of  $V$ , and should be able to discriminate between large-scale rotation (NGC 3379) and little or no rotation (NGC 5813). Such a quantity, however, depends on the determination of the angular momentum vector direction, which is not an easily measured quantity. We therefore use a more robust and measurable quantity  $\langle R|V| \rangle$ , where  $R$  is the observed distance to the galactic centre, as a surrogate for  $L$ , and the brackets  $\langle \rangle$  correspond to a luminosity-weighted sky average (see equation 2). We can then naturally define a dimensionless parameter, after normalizing by, for example, mass, which leads to a proxy for the *baryon* projected specific angular momentum as

$$\lambda_R \equiv \frac{\langle R|V| \rangle}{\langle R \sqrt{V^2 + \sigma^2} \rangle}, \quad (5)$$

and measured via two-dimensional spectroscopy as

$$\lambda_R = \frac{\sum_{i=1}^{N_p} F_i R_i |V_i|}{\sum_{i=1}^{N_p} F_i R_i \sqrt{V_i^2 + \sigma_i^2}}, \quad (6)$$

where  $F_i$  is the flux inside the  $i$ th bin,  $R_i$  its distance to the centre, and  $V_i$  and  $\sigma_i$  the corresponding mean stellar velocity and velocity dispersion. The normalization by the second velocity moment  $V^2 + \sigma^2$  implies that  $\lambda_R$  goes to unity when the mean stellar

rotation ( $V$ ) dominates, with  $V^2 + \sigma^2$  being a reasonable proxy for mass (see Appendix A). The use of higher-order moments of either  $V$  or the spatial weighting  $R$  would make this parameter more strongly dependent on the aperture and presence of noise in the data.  $\lambda_R$  obviously depends on the spatial extent over which the sums in equation (6) are achieved. In practice, we measure  $\lambda_R(R_m)$  within regions defined by the photometric best-fitting ellipses, where  $R_m$  is the mean radius of that ellipse ( $a\sqrt{1-\epsilon}$ , with  $a$  its semimajor axis and  $\epsilon$  its ellipticity), the area  $A_{\text{ellipse}}$  of the corresponding aperture being thus  $\pi R_m^2$ , the area of a circle with a radius of  $R_m$ . When our SAURON kinematic measurements do not fully sample the defined ellipse, we instead set the radius  $R_m \equiv \sqrt{A_S/\pi}$  as that of a circular aperture with the same area  $A_S$  on the sky actually covered by the SAURON data inside that aperture (see Paper IV). For a specific galaxy, we measure  $\lambda_R(R_m)$  up to the radius for which we reach a maximum difference of 15 per cent between  $A_S$  and  $A_{\text{ellipse}}$ : this guarantees that the SAURON kinematic data still properly fill up the elliptic aperture defined by the photometry.

### 3.2 Rotators and $\lambda_R$

Values of  $\lambda_{R_c}$ ,  $\lambda_R$  within  $1R_c$  or the largest radius allowed by our SAURON data, whichever is smaller, are provided in Table 1 for the 48 E/S0 galaxies. As expected, NGC 3379 and 5813, which have similar  $V/\sigma$  values (see Fig. 1 and Section 3.1) but *qualitatively* different velocity structures, are now *quantitatively* distinguished with  $\lambda_{R_c}$  values of 0.14 and 0.06, respectively. This difference is significant because the formal uncertainty in the derivation of  $\lambda_{R_c}$  due to the presence of noise in the data is almost always negligible, and any smaller than 0.02 for galaxies such as NGC 3379 and 5813 (Appendix B): this can be understood because  $\lambda_{R_c}$  includes averages over a large area. There is, however, a systematic (positive) bias which obviously increases as the velocity amplitudes in the galaxy decrease, and can reach up to about 0.03 in the measurement of  $\lambda_{R_c}$ . This bias is therefore dominant for the three galaxies with very low  $\lambda_{R_c}$  ( $< 0.03$ ), the mean stellar velocities being in fact consistent with zero values everywhere in the field of view.

As we go from galaxies with low to high  $\lambda_{R_c}$  values, the overall velocity amplitude naturally tends to increase. More importantly, there seems to be a *qualitative* change in the observed stellar velocity structures. This is already illustrated in Fig. 1, where the 48 SAURON stellar velocity fields are ordered, from left to right, top to bottom, by increasing value of  $\lambda_{R_c}$ . Rotators with  $\lambda_{R_c} < 0.1$  exhibit low stellar mean velocities at large radii, with very perturbed stellar kinematics and large-scale KDCs (this point will be further examined in Section 4.4).

This qualitative change is nicely illustrated in Fig. 2 where we show the radial  $\lambda_R$  profiles. Galaxies with  $\lambda_{R_c}$  below and above 0.1 exhibit qualitatively very different  $\lambda_R$  profiles: the former have either decreasing or nearly flat (and small amplitude)  $\lambda_R$  profiles, while the latter preferentially exhibit significantly increasing  $\lambda_R$  radial profiles. Observed  $\lambda_R$  gradients are therefore negative or rather small within  $1R_c$  for galaxies with  $\lambda_{R_c} < 0.1$ , and we will label them as ‘slow rotators’. This contrasts with the significantly rising  $\lambda_R$  profiles for galaxies with  $\lambda_{R_c} > 0.1$ , which all exhibit clear large-scale and relatively regular rotation patterns, and which we label, by opposition, as ‘fast rotators’: the fact that this class includes both mild and very fast rotators is discussed in Section 3.4.

As mentioned, Table 1 includes  $\lambda_{R_c}$  values derived using the SAURON two-dimensional kinematic maps available and a default equivalent aperture of  $1R_c$ . This aperture is in fact covered by the SAURON datacubes for 17 galaxies out of the 48 in the SAURON

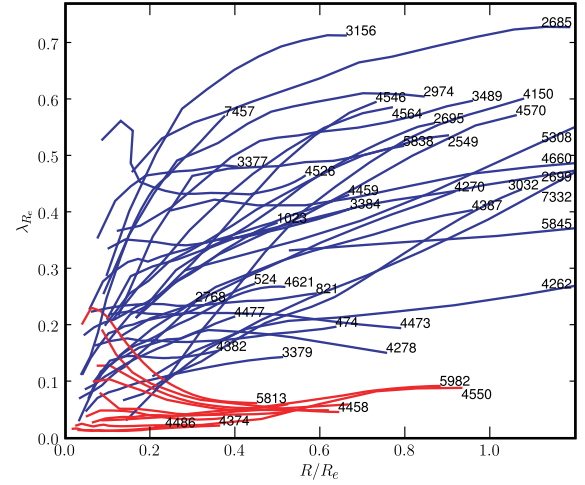


**Figure 2.** Radial  $\lambda_R$  profiles for the 48 E and S0 galaxies of the SAURON sample. Profiles of slow and fast rotators are coloured in red and blue, respectively. NGC numbers are indicated for all fast rotators and most slow rotators (a few were removed for legibility).

E/S0 sample (see Paper IV), with two galaxies being mapped only to  $\sim 0.3R_c$  (NGC 4486 and 5846). Galaxies with the narrowest relative spatial coverage (with the largest  $R_c$ : NGC 4486, 5846) are among the slowest rotators of our sample: these two galaxies are in fact known not to exhibit any significant rotation within  $1R_c$  (see Sembach & Tonry 1996), even though NGC 4486 (M 87) is in fact flattened at very large radii (see Kissler-Patig & Gebhardt 1998, and references therein). This implies that only a few galaxies near the  $\lambda_{R_c} = 0.1$  threshold (NGC 5982, 4550, 4278) could cross that threshold if we were to have a complete coverage up to  $1R_c$ .

This is also illustrated in Fig. 3 which shows that histograms of  $\lambda_{R_c}$  for radii of  $1R_c$  and  $R_c/2$  (or restricted to the equivalent effective aperture of the SAURON field of view, whichever is smaller) have the same fraction of slow and fast rotators. The overall distribution of  $\lambda_R$  values is similar for  $R_c$  and  $R_c/2$ , although  $\lambda_R$  tends to increase significantly from  $R_c/2$  to  $R_c$  for fast rotators (see also the solid straight lines in Fig. 5), an obvious implication of the observed rising  $\lambda_R$  profiles in Fig. 2. There are 36 fast rotators and 12 slow

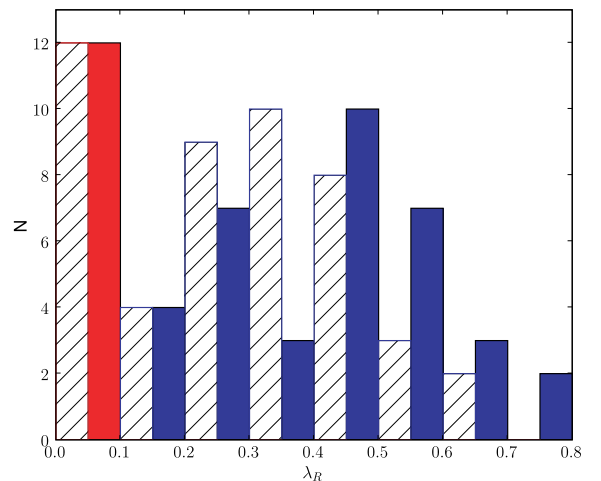


**Figure 3.** Histogram of  $\lambda_R$ : bars with plain colours correspond to  $\lambda_{R_c} \equiv \lambda_R(R_c)$  and the dashed bars to  $\lambda_R(R_c/2)$ . Red bars indicate the  $\lambda_R$  bin for slow rotators: the number of slow rotators does not change if we were to measure  $\lambda_R$  at  $R_c/2$ .

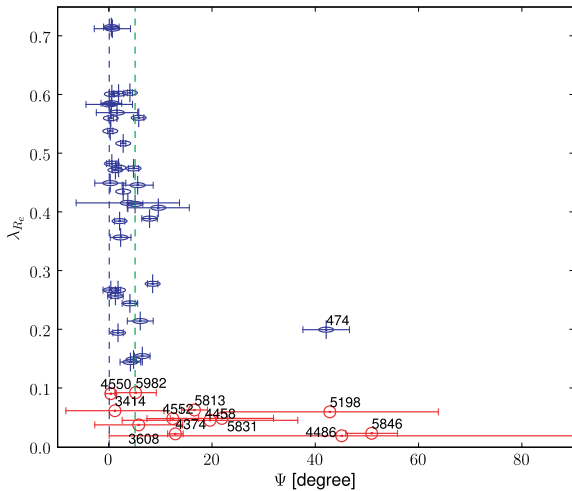


**Figure 4.**  $\lambda_{R_c}$  versus the KM  $\Psi$  between the global photometric major axis and the kinematic axis within the SAURON field. Slow rotators are represented by red circles and fast rotators by special blue symbols (horizontal ellipse plus a vertical line). The vertical dashed line corresponds to  $\Psi = 5^\circ$ . Nearly all fast rotators have small  $\Psi$  values ( $< 10^\circ$ ), the only exception being NGC 474, the photometry of which is perturbed by the presence of irregular shells. This contrasts with slow rotators which show significantly non-zero  $\Psi$  values.

rotators (75 and 25 per cent of the total sample), their median  $\lambda_{R_c}$  values being  $\sim 0.44$  and  $0.05$ , respectively. Within the class of slow rotators, three galaxies have  $\lambda_{R_c}$  significantly below  $0.03$  (their mean stellar velocity maps being consistent with zero rotation everywhere, as mentioned above). These are among the brightest galaxies of our sample, namely NGC 4486, 4374 and 5846.

### 3.3 Misalignments and twists

The fact that slow and fast rotators exhibit distinct kinematics can be demonstrated by considering the global alignment (or misalignment) between photometry and kinemetry. Fig. 4 illustrates this by showing the KM  $\Psi \equiv |\text{PA}_{\text{phot}} - \text{PA}_{\text{kin}}|$  for all 48 E and S0 galaxies in the SAURON sample. Note that the photometric PA is derived using the large-scale MDM data, but the kinematic PA via a global measurement on the SAURON velocity maps as described in appendix C of Krajnović et al. (2006). All fast rotators, except one, have misalignments  $\Psi$  below  $10^\circ$ . The only exception is NGC 474 which is an interacting galaxy with well-known irregular shells (Turnbull, Bridges & Carter 1999). In fact, the few galaxies which have  $5^\circ < \Psi < 10^\circ$  (NGC 3377, 3384, 4382, 4477, 7332) are almost certainly barred. Even the two relatively face-on galaxies, NGC 4262 and 4477, the photometry of which shows the signature of a strong bar within the SAURON field of view, have their *outer* photometric PA well aligned with the measured kinematic PA. In contrast, more than half of all slow rotators have  $\Psi > 10^\circ$ , and none of these exhibits any hint of a bar. This difference in the misalignment values of slow and fast rotators cannot be entirely due to the effect of inclination, not only because of the argument mentioned in Section 4.2, but also because even the roundest fast rotators do not exhibit large misalignment values (see section 5.1 in Paper X).

Another remarkable feature comes from the observed velocity twists in the SAURON kinematic maps: only six galaxies out of 48 exhibit strong velocity twists larger than  $30^\circ$  outside the inner 3 arcsec, namely NGC 3414, 3608, 4550, 4552, 5198 and 5982, with three out of these six having large-scale counter-rotating stellar

components (NGC 3414, 3608 and 4550). All these galaxies are in fact slow rotators. This implies that only fast rotators have a relatively well-defined (apparent) kinematic major axis, which in addition is roughly aligned with the photometric major axis.

There is a close link between  $\lambda_R$  and the (apparent) specific angular momentum (see Appendix A).  $\lambda_R$  is therefore a continuous parameter which provides a *quantitative* assessment of the apparent mean stellar rotation. As emphasized in this section, slow and fast rotators exhibit quantitatively but also qualitatively different stellar kinematics. This strongly suggests that slow rotators as a class cannot simply be scaled-down versions of galaxies with  $\lambda_{R_c} > 0.1$ .

### 3.4 Inclination effects

Obviously,  $\lambda_R$  is derived from projected quantities and therefore also significantly depends on the viewing angles. Can slow rotators be face-on versions of fast rotators? Assuming  $\lambda_R$  roughly follows the behaviour of  $V/\sigma$  with the inclination angle  $i$  (Appendix B), a galaxy with a *measured*  $\lambda_{R_c} = 0.05$ , typical of observed slow rotators, would require to be at a nearly face-on inclination of  $i \sim 20^\circ$  to reach an *intrinsic* (edge-on) value of  $\lambda_{R_c} \sim 0.15$ , the smallest value for all observed fast rotators in our sample. The probability that slow rotators are truly fast rotators seen face-on is therefore small, and cannot explain the 25 per cent population of slow rotators observed in the  $\lambda_{R_c}$  histogram (Fig. 3).

As emphasized above, the measured  $\lambda_{R_c}$  values are most probably lower limits because we observe galaxies away from edge-on. An illustrative example is provided by the case of NGC 524. According to Paper IV, NGC 524 is viewed with an inclination of  $19^\circ$ : still, NGC 524 exhibits a regular velocity pattern, and is a fast rotator with  $\lambda_{R_c} \sim 0.28$ . There is also some evidence that the three fast rotators with the lowest  $\lambda_{R_c}$  values in our sample, namely NGC 3379, 4278 and 4382, are significantly inclined galaxies (Fisher 1997; Statler 2001; Paper III; Paper IV; Sarzi et al. 2006, hereafter Paper V). This illustrates the fact that the apparent distribution of  $\lambda_{R_c}$  *within* the fast rotator class may not fully reflect the intrinsic distribution with galaxies viewed edge-on. It is, however, impossible to estimate the ‘edge-on’  $\lambda_{R_c}$  distribution for fast rotators as this would require *ad minima* an accurate measurement of their inclination. Although the fast rotator class may probably include truly mild as well as very fast rotators (as expected from the continuous nature of  $\lambda_{R_c}$ ), all galaxies with  $\lambda_{R_c} > 0.1$  exhibit a global and regular rotation pattern, with a clear sense of rotation and a significant amount of specific stellar angular momentum. This, to us, justifies the use of the label ‘fast rotators’ for these galaxies. Further discussions of the true nature of fast rotators as a class has to wait for a larger and complete sample.

## 4 OTHER CLASSIFICATIONS

In this section, we examine in more detail other galaxy properties, including photometry and kinemetry, to determine if these could help in defining kinematic classes, and their potential link with  $\lambda_R$ .

### 4.1 Hubble Classification

There is a clear overlap of Es and S0s in the fast rotator class, with most of the corresponding galaxies having ellipticities higher than  $0.2$ . This illustrates the fact that many Es have kinematic characteristics similar to S0s (Bender 1988; Rix & White 1990). Some galaxies classified as Es also show photometric signatures of embedded discs, quantified as a positive  $a_4/a$ , and were classified as



‘discy’ Es or E(d) by KB96. It seems difficult, however, to distinguish between a so-called E(d) and a S0 galaxy from the photometric properties or the anisotropy diagram alone. KB96 argued that E(d)s are objects intermediate between S0s and boxy Es or E(b)s (Es with boxy isophotes, i.e. negative  $a_4/a$ ). In principle, the Ed–S0–Sa sequence is one of decreasing bulge-to-total light ratio (B/T), with S0s having  $B/T \sim 0.6$  in the  $B$  band (Fritze v. Alvensleben 2004). B/T is, however, a fairly difficult quantity to measure in early-type galaxies, as it depends on the adopted model for the surface brightness distribution of the disc and bulge components. As emphasized by de Jong et al. (2004a), the kinematic information is critical in assessing the rotational support of both components.

Consider two galaxies of our sample, NGC 3377 and 2549, both of which have similar  $\lambda_{R_e}$ , the former being classified as a discy E and the latter as a S0. Both have very similar total luminosity,  $V - I$  colour (Tonry et al. 2001) and gas content (Paper V). Their SAURON stellar kinematic maps are also quite similar (Paper III), with large-scale disc-like rotation, a centrally peaked stellar velocity dispersion and a significant  $h_3$  term, anticorrelated with the mean velocity. Finally, there is evidence that NGC 3377 contains a bar, with its velocity map exhibiting a stellar kinematical misalignment (KM) and a spiral-like ionized gas distribution (Paper V). This therefore strongly argues for NGC 3377 to be a misclassified barred S0 (SAB0). Many authors (e.g. van den Bergh 1990; Jorgensen & Franx 1994; Michard 1994, KB96) indeed suggested that many Es are in fact misclassified S0s, mostly on the basis of photometry alone. Considering the kinematic properties of the observed SAURON early-type galaxies, we suspect that most and possibly all of the 13 Es which are fast rotators are in fact misclassified S0 galaxies, a conclusion also supported by the results of Paper X via the use of state-of-the-art dynamical models.

## 4.2 Isophote shapes

Fig. 5 shows  $\lambda_{R_e}$  versus the global ellipticity  $\epsilon$  for the 48 SAURON E and S0s, measured using an aperture of  $1R_e$  (or including the full SAURON field of view for galaxies with large  $R_e$ ; see Section 3.2).

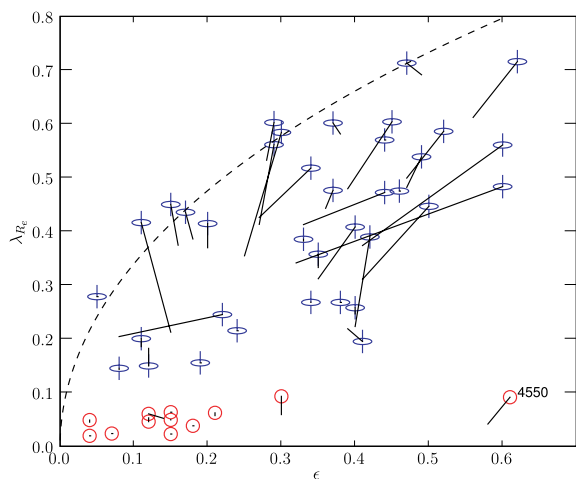


**Figure 5.**  $\lambda_{R_e}$  versus the global ellipticity  $\epsilon$  for the 48 E and S0 galaxies of the SAURON sample. The solid lines indicate where the points would move for a smaller equivalent effective aperture of  $R_e/2$ . Slow rotators (which have  $\lambda_{R_e} \leq 0.1$ ) are red circles, and fast rotators ( $\lambda_{R_e} > 0.1$ ) are represented by special blue symbols (horizontal ellipse plus a vertical line). The black dashed line corresponds to the curve expected for isotropic oblate rotators viewed edge-on (see Appendix B and Binney 2005). The galaxy NGC 4550 is labelled.

All galaxies in Fig. 5 lie close to or below the curve expected for isotropic oblate rotators viewed edge-on (see Appendix B and Binney 2005). Fast rotators, which have velocity maps with significant large-scale rotation, have ellipticities ranging up to about 0.6. Apart from the atypical case of NGC 4550, slow rotators show little or spatially confined rotation and all have ellipticities  $\epsilon < 0.3$ . NGC 4550 is in fact a nearly edge-on galaxy with two co-spatial counter-rotating stellar discs, each contributing for about 50 per cent of the total luminosity, and should therefore be regarded as an atypical case where a high ellipticity is accompanied by a relatively low mean stellar velocity in the equatorial plane (Rix et al. 1992; Rubin, Graham & Kenney 1992, and see Paper X for a detailed discussion).

KB96 mention that  $a_4/a$  can be used as a reasonably reliable way to measure velocity anisotropy. They first observe, using  $(V/\sigma)^*$  ( $V/\sigma$  normalized to the value expected for an isotropic edge-on oblate system), that discy galaxies ( $a_4/a > 0$ ) seem consistent with near isotropy, whereas boxy galaxies ( $a_4/a < 0$ ) spread over a large range of  $(V/\sigma)^*$  values. However, as emphasized by Binney (2005) and in Paper X,  $(V/\sigma)^*$  is not a good indicator of anisotropy: the relation between  $(V/\sigma)^*$  and the anisotropy of a galaxy strongly depends on its flattening, as well as on its inclination (Burkert & Naab 2005). More flattened galaxies will thus tend to lie closer to the  $(V/\sigma)^* = 1$  curve, which explains in part why galaxies with discy and boxy isophotes seem to extend over different ranges of  $(V/\sigma)^*$ , the former being then incorrectly interpreted as near-isotropic systems. This suggests we should avoid using  $(V/\sigma)^*$  at all, and leads us to examine more directly the orbital anisotropy of galaxies (see Binney 2005). This is achieved in Paper X, in which a trend between the anisotropy parameter in the meridional plane and the average intrinsic ellipticity is revealed (see their fig. 7), intrinsically more *flattened* galaxies tending to be more *anisotropic*. This contradicts the view that discy galaxies are nearly isotropic, and we should therefore reexamine the relation between the isophotal shape as measured by  $a_4/a$  and the kinematic status of early-type galaxies. KB96 presented a fairly significant correlation between the mean ellipticity  $\epsilon$  and  $a_4/a$  for their sample of early-type galaxies (their fig. 3). They mentioned that galaxies in a  $\epsilon$  versus  $a_4/a$  diagram exhibit a V-shaped distribution. The authors therefore pointed out that this remarkable correlation implies that early-type galaxies with nearly E isophotes are also nearly round, and galaxies with the most extreme  $a_4/a$  values are also the most flattened (see also Hao et al. 2006). We confirm this result using our photometric data on the SAURON sample as shown in Fig. 6 (upper panel). As mentioned above, all slow rotators with the exception of NGC 4550 have ellipticities  $\epsilon_e$  lower than 0.3, and our expectation that these galaxies should have isophotes close to pure ellipses is verified: 10 out of 11 have  $|(a_4/a)_e| < 1$  per cent [with nine out of 11 having  $|(a_4/a)_e| < 0.5$  per cent], the exception being NGC 3414, for which the relatively large positive  $(a_4/a)_e$  value comes from the remarkable polar-ring structure (van Driel et al. 2000).

In fact, most fast rotators have a *maximum* absolute  $|(a_4/a)|$  value within  $1R_e$  larger than 2 per cent, whereas most slow rotators (with the exceptions again of NGC 3414 and 4550) have *maximum* absolute  $|(a_4/a)|$  values less than 2 per cent. This means that most fast rotators in the SAURON sample of E and S0 galaxies exhibit significantly non-E isophotes, but most slow rotators do not. There is a tendency for the fast rotators to have positive  $a_4/a$  (discy isophotes), and most slow rotators (seven out of 12) have negative  $a_4/a$  (boxy isophotes). We do not detect any global and significant correlation between the boxiness and the angular momentum per unit mass as quantified by  $\lambda_{R_e}$  in the galaxies of our sample, so that  $|(a_4/a)|$  is

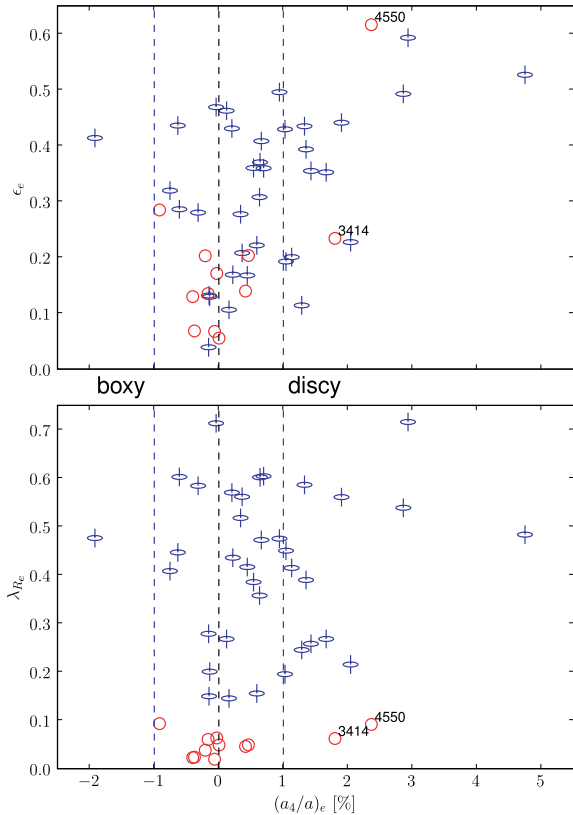


**Figure 6.** Mean ellipticity  $\epsilon_e$  (top) and  $\lambda_{R_e}$  (bottom) versus mean  $(a_4/a_e)$  (in per cent) within  $1R_e$ . Symbols for slow and fast rotators are as in Fig. 5. The vertical dashed lines correspond to  $(a_4/a_e) = \pm 1$  per cent.

clearly not a good proxy for rotation or angular momentum. This seems partly in contradiction with the claim by KB96 that rotation is dynamically less important in boxy than in discy early-type galaxies. The latter result probably originated from the combination of two observed facts: first boxy galaxies are on average less flattened (extremely flattened galaxies are very discy), and secondly the use of  $(V/\sigma)^*$  as a proxy for the amount of organized rotation in the stellar component, which tends to underestimate the rotational support for less flattened galaxies.

### 4.3 Luminosity and mass

In the left-hand panel of Fig. 7, we show the distribution of  $\lambda_{R_e}$  as a function of absolute magnitude  $M_B$  for the 48 SAURON E/S0 galaxies. The three slowest rotators (NGC 4486, 4374, 5846) are among the brightest galaxies in our sample with  $M_B < -21$  mag. Other slow rotators tend to be bright but are spread over a wide range of absolute magnitude going from the relatively faint NGC 4458 to brighter objects such as NGC 5813. The bright and faint end of slow rotators can be distinguished by the shapes of their isophotes: slow rotators brighter than  $M_B < -20$  mag all exhibit mildly boxy isophotes (negative  $a_4/a$  with amplitude less than 1 per cent) while the four discy slow rotators are all fainter than  $M_B > -20$  mag, following the known correlation between the isophote shapes and the total luminosity of early-type galaxies (Bender, Burstein & Faber 1992). Most fast rotators are fainter than  $M_B > -20.5$  mag.

Going from total luminosity to mass, we have estimated the latter by approximating it with the virial mass  $M_{\text{vir}}$  derived from the best-fitting relation obtained in Paper IV, namely  $M_{\text{vir}} \sim 5.0 R_e \sigma_e^2 / G$ ,

where  $\sigma_e$  is the luminosity-weighted second velocity moment within  $1R_e$  (see Paper IV for details). The calculation of  $M_{\text{vir}}$  from observables depends on the distance of the object, which we obtained from different sources for the galaxies in our sample (in order of priority, from Tonry et al. 2001; Tully 1988, and from the LEDA data base assuming a Hubble flow with  $H = 75 \text{ km s}^{-1} \text{ Mpc}^{-1}$ ). A trend of  $\lambda_{R_e}$  tending to be lower for more massive galaxies clearly emerges if we now use this estimate of the virial mass  $M_{\text{vir}}$  (right-hand panel of Fig. 7), as expected from the one observed with absolute magnitude  $M_B$  (left-hand panel of Fig. 7). The three slowest rotators are in the high range of  $M_{\text{vir}}$  with values above  $10^{11.5} M_{\odot}$ . There is a clear overlap in mass between fast and slow rotators for  $M_{\text{vir}}$  between  $10^{11}$  and  $10^{11.5} M_{\odot}$ . However, all slow rotators, besides NGC 4458 and 4550, have  $M_{\text{vir}} > 10^{11} M_{\odot}$ , whereas most fast rotators have  $M_{\text{vir}} < 10^{11} M_{\odot}$ , lower masses being reached as the value of  $\lambda_{R_e}$  increases. It is worth pointing out that the absolute magnitude in the  $K$  band,  $M_K$ , very nicely correlates with  $M_{\text{vir}}$  (significantly better than with  $M_B$ ), so that the trend observed between  $\lambda_{R_e}$  and  $M_{\text{vir}}$  is also observed if we were to examine the relation between  $\lambda_{R_e}$  and  $M_K$ .

Out of the 48 SAURON galaxies, 33 have published cusp slope classification, distinguishing ‘core’ and ‘power-law’ galaxies (Faber et al. 1997; Ravindranath et al. 2001; Rest et al. 2001; Lauer et al. 2005). As illustrated in the left-hand panel of Fig. 7, we find that most slow rotators are core galaxies, and most fast rotators are power-law galaxies (note that NGC 821 has an  $\lambda_{R_e} \sim 0.25$  and is specified as an ‘intermediate’ object between a core and power law in Lauer et al. 2005). There are yet no core galaxies with  $\lambda_{R_e} > 0.3$ , although the inclined galaxy NGC 524 (see Paper IV) would have a very high  $\lambda_{R_e}$  value if seen edge-on. These results are expected as there is a known trend between the central luminosity gradient and the total luminosity of early-type galaxies, bright members tending to be core galaxies, and lower luminosity ones to have power-law profiles (Faber et al. 1997). All galaxies with  $\lambda_{R_e} > 0.3$  have indeed  $M_B > -20.7$  and conversely none has  $M_{\text{vir}} > 10^{11.5} M_{\odot}$ . This is, however, not a one-to-one correspondence since we find both power law in slow rotators (NGC 3414 and 5813) and core-like fast rotator (e.g. NGC 524). There is also a domain in mass and luminosity where both cusps and cores are found, namely for  $M_{\text{vir}}$  between  $10^{11}$  and  $10^{11.5} M_{\odot}$ , or correspondingly for  $M_B$  from  $-19.5$  to  $-20.5$ . Another interesting result is found when examining the larger-scale luminosity profiles of galaxies in our sample via the representation by a Sersic law. Besides the atypical case of NGC 4550, all slow rotators have Sersic index  $n > 4$ : again, this is expected since galaxies with larger Sersic shape index tend to be brighter (Caon, Capaccioli & D’Onofrio 1993; Graham & Guzmán 2003). Finally, galaxies with the lowest Sersic  $n$  values are also among the fastest rotators. A more detailed account regarding these issues will be provided in Falc3n-Barroso et al. (in preparation).

### 4.4 Kinemetry groups

We now turn to the kinematic profiles (see Section 2.4) of the 48 SAURON galaxies, which allow us to determine the number of observed kinematic components and their individual characteristics. We thus make use of the average photometric and kinematic position angles and axis ratio ( $\text{PA}_{\text{phot}}$  and  $\text{PA}_{\text{kin}}$ ,  $q$  and  $q_{\text{kin}}$ ), and the average and maximum of the velocity amplitude  $k_1$ .

The kinematic groups of the observed 48 SAURON velocity maps, defined in Section 2.4, are provided in Table 1. Out of 48 galaxies in this sample, 33 (69 per cent) exhibit MC, including 10 KDCs (21 per cent) and four objects with CLVs (namely NGC 3032, 4150, 4382 and 7457). Two more galaxies with KDCs

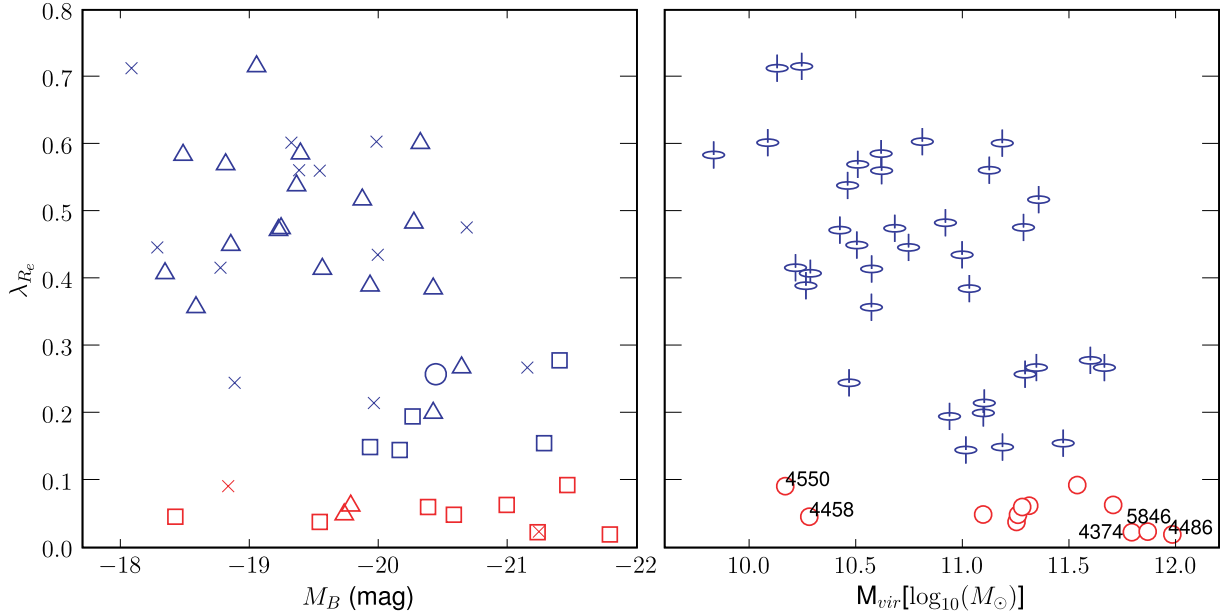


**Figure 7.**  $\lambda_{R_e}$  versus absolute magnitude  $M_B$  (left-hand panel) and virial mass  $M_{vir}$  (right-hand panel) for the 48 E and S0 of the SAURON sample. In the left-hand panel, symbols correspond to the cusp slope classification (Faber et al. 1997; Ravindranath et al. 2001; Rest et al. 2001; Lauer et al. 2005) with power laws as triangles, cores as squares, NGC 821 which is an ‘intermediate’ object as a circle, and crosses indicating galaxies for which there is no published classification. In the right-hand panel, symbols for slow and fast rotators are as in Fig. 5, and NGC numbers for a few galaxies are indicated.

are in fact at the limit of being CLVs (NGC 4621 and 7332) with a maximum velocity for their inner component around  $20 \text{ km s}^{-1}$  at the SAURON resolution. The latter two galaxies as well as the CLVs have in fact all been shown to harbour small counter-rotating stellar systems (Wernli, Emsellem & Copin 2002; Falcón-Barroso et al. 2004; McDermid et al. 2006, hereafter Paper VIII); it is the lower spatial resolution of the SAURON data which produces the low central velocity gradient. If we therefore count CLVs as galaxies with KDCs, this would result in a total of 14 KDC (29 per cent) early-type objects. Among the KDCs, five galaxies (NGC 3414, 3608, 4458, 5813 and 5831) have outer LV components. KMs are observed in 12 galaxies (25 per cent), and six galaxies have individual kinematic components which have KT (two of them also having KM). Considering the difficulty of detecting these structures at certain viewing angles or low spatial resolution, the number of such detected velocity structures is a lower limit.

In Fig. 8, we show the  $(\lambda_{R_e}, \epsilon)$  diagram (as in Fig. 5), now with the characteristic velocity structures detected via kinemetry. The three slowest rotators are obviously tagged as low-velocity (LV) systems. As mentioned above, these three galaxies are giant (bright and massive) roundish Es with  $M_B < -21$ . Apart from these three and the atypical case of NGC 4550, all other slow rotators harbour KDCs, the central kinematic component having a typical size of 1 kpc or larger (see Paper VIII). This contrasts with KDCs and CLVs in fast rotators (NGC 3032, 4150, 7332, 7457), where the size of the central (counter-rotating) stellar component is only a few arcsec in radius, corresponding to significantly less than 500 pc (Paper VIII).

A number of fast rotators show KM and twists (KT), most of these being relatively small in contrast with the ones found in slow rotators (see Section 3.3). The four fastest rotators with a KT, KM or KDC, namely NGC 1023, 3377, 7332 and 7457, are all barred galaxies. Most of the galaxies with multicomponents but no specific velocity structures are among the fastest rotators. This result may be partly understood if these objects tend to be close to edge-on,

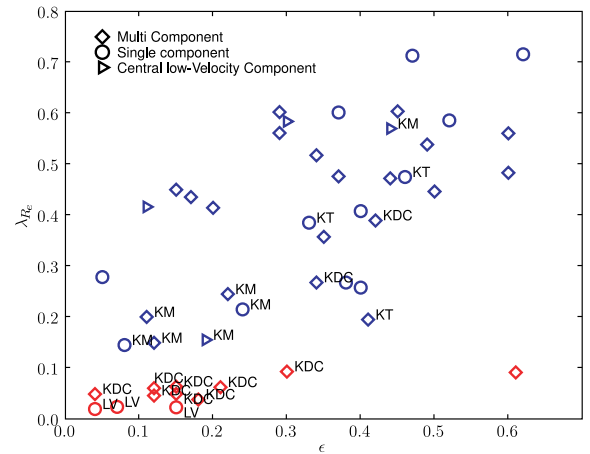


**Figure 8.**  $\lambda_{R_e}$  versus mean ellipticity  $\epsilon$ , with indications of the velocity structures identified in Section 2.4. Galaxies with MCs are shown as diamonds, SCs as circles and CLVs as right triangles. Colours for slow and fast rotators are as in Fig. 5. KDC stands for kinematically decoupled components, KM and KT for Kinematic misalignment and twist, respectively, and LV for low-velocity component.

which renders the detection of such velocity structures harder, but the detection of MCs easier.

## 5 DISCUSSION

The fast rotators are mostly discy galaxies exhibiting MCs in their stellar velocity fields. Contrarily to slow rotators, the main stellar kinematic axis in fast rotators is relatively well aligned with the photometric major axis, except for one galaxy (NGC 474) known to harbour irregular shells. This result together with the fact that the  $\lambda_R$  profiles are qualitatively different for slow and fast rotators clearly

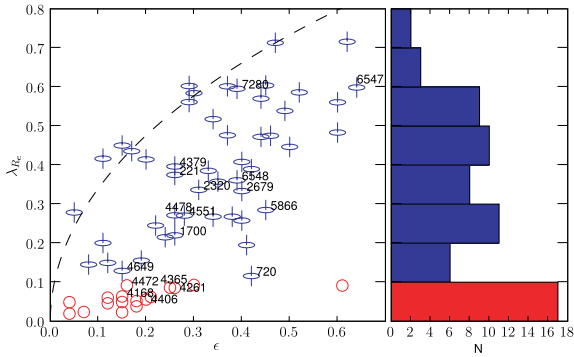


**Figure 9.** Left-hand panel:  $\lambda_{Rc}$  versus the ellipticity  $\epsilon$  including the additional 18 E and S0 galaxies observed with SAURON (labelled with NGC numbers). Symbols and the dashed line are as in Fig. 5. Right-hand panel: histogram of  $\lambda_{Rc}$  values including the 18 ‘specials’.

shows that slow rotators are not velocity scaled-down versions of fast rotators. The small number of galaxies in our sample, as well as our biased representation of the galaxy luminosity function, reminds us that a larger and complete sample is required to reveal the true  $\lambda_{Rc}$  distribution in early-type galaxies.

We therefore first briefly discuss here the results obtained so far, this time including 18 additional early-type galaxies (‘specials’) observed with SAURON within the course of other specific projects. For these additional targets, we had to retrieve the main photometric parameters (e.g.  $R_e$ ,  $\epsilon$ ,  $a_4/a$ ) from the literature (e.g. Bender et al. 1988; Faber et al. 1997), the kinematic measurements ( $\sigma_e$ ,  $\lambda_{Rc}$ ) being derived from the available SAURON data as for the 48 E/S0 galaxies of the main sample (only 12 galaxies out of the 18 specials have available  $a_4$  measurements). Adding these 18 galaxies does not change the overall distribution of fast and slow rotators in a  $\lambda_{Rc}$  versus  $\epsilon$  diagram, as shown in Fig. 9. The fraction of slow rotators (17 out of 66) is still  $\sim 25$  per cent. We also confirm that most slow rotators have relatively small ellipticities ( $\epsilon < 0.3$ ), in contrast with fast rotators which span a wide range of flattening. The most remarkable fact lies in the confirmation that within these 18 extra targets, there are five slow rotators (NGC 4168, 4406, 4472, 4261 and 4365), and they *all* contain large (kpc) scale KDCs. Similarly, in Fig. 10 we confirm the lack of a global significant correlation

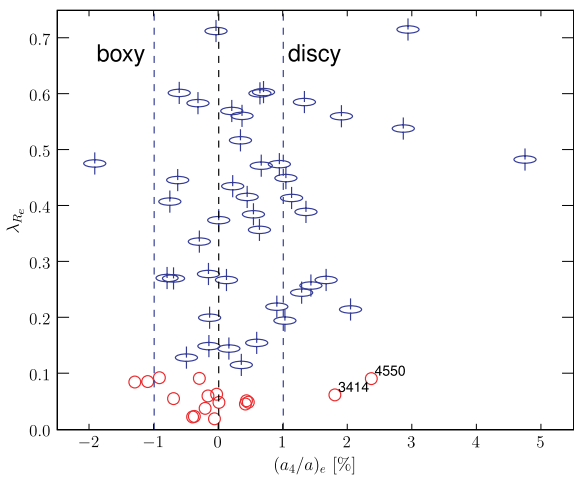


**Figure 10.**  $\lambda_{Rc}$  versus  $a_4$  for the 48 E/S0 of the SAURON sample and an additional 12 galaxies for which we have available  $a_4$  values. Symbols for slow and fast rotators are as in Fig. 6.

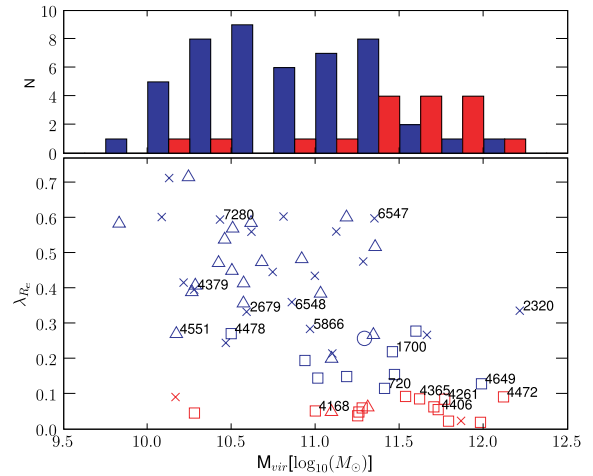


**Figure 11.**  $\lambda_{Rc}$  versus the virial mass  $M_{\text{vir}}$  for the 48 E/S0 of the SAURON sample plus an additional 17 ‘specials’ (we do not include the fast rotator NGC 221 – M 32 – in this plot considering its very low mass). The top panel shows histograms of  $M_{\text{vir}}$  (in log, with steps of 0.5) for both slow (red) and fast rotators (blue). Colours in both panels for slow and fast rotators are as in Fig. 6. NGC numbers are indicated for all specials. Symbols for galaxies with cores and cusps are as in the left-hand panel of Fig. 7.

between  $\lambda_{Rc}$  and  $a_4/a$  as shown in Fig. 6. Again, about two-thirds of the slow rotators are boxy (five out of 17 are discy and one has  $a_4/a = 0$ ), and very discy galaxies tend to be fast rotators with high  $\lambda_{Rc}$  values. However,  $a_4/a$  is clearly not a good proxy for angular momentum. We then show in Fig. 11 the relation between  $\lambda_{Rc}$  and  $M_{\text{vir}}$  with an additional 17 ‘specials’ (excluding the compact galaxy NGC 221 [M 32] which would stretch the plot unnecessarily). Most slow rotators are massive galaxies with  $M_{\text{vir}} > 10^{11} M_{\odot}$ , with still only two exceptions (NGC 4550 and 4458), reinforcing the results from Fig. 11. The trend for more massive galaxies to have lower  $\lambda_{Rc}$  values is still observed, with an overlap of fast and slow rotators in the range  $10^{11} - 10^{12} M_{\odot}$ . The fast rotator NGC 2320 seems to have a rather large  $\lambda_{Rc}$  for its virial mass (being in fact the most massive galaxy out of the 66). NGC 2320 is the most distant galaxy of this set (with  $D \sim 83$  Mpc), and has a rather unusual molecular gas content for an early-type galaxy: it exhibits an asymmetric molecular gas disc with a mass of about  $4 \times 10^9 M_{\odot}$ , interpreted as a sign of recent accretion or dynamical perturbation (Young 2005).

In Fig. 11, we also show the ‘cusp/core’ classification as in Section 4.3. Most fast rotators are still galaxies with cusps, and most slow rotators are core galaxies. Conversely, massive galaxies tend to have cores, and smaller ones tend to exhibit cuspy central luminosity profiles: in fact, all galaxies with  $M_{\text{vir}} > 10^{11.5} M_{\odot}$  have cores. There is a transition region, in the range  $10^{11} - 10^{11.5} M_{\odot}$  where we find both cusp and core galaxies. More interestingly, all core galaxies still have  $\lambda_{Rc} < 0.3$ . However, a galaxy like NGC 524 is almost certainly very inclined (see Paper IV), its corresponding ‘edge-on’  $\lambda_{Rc}$  value being then much larger than 0.75. It would thus be interesting to understand if an edge-on version of NGC 524 would still have a core-like central luminosity profile. We also observe a few galaxies with cusps and rather low  $\lambda_{Rc}$  values (NGC 5831) which cannot be reconciled with inclined fast rotators. We may therefore only discriminate cusp and core galaxies combining both their mass *and* their  $\lambda_{Rc}$  values: massive galaxies ( $M_{\text{vir}} > 10^{11.5} M_{\odot}$ ) with  $\lambda_{Rc} < 0.3$  are indeed all core galaxies, while smaller galaxies ( $M_{\text{vir}} < 10^{11} M_{\odot}$ ) with  $\lambda_{Rc} > 0.3$  seem to all be galaxies with



cusps. The fact that we observe very few massive ( $M_{\text{vir}} > 10^{11} M_{\odot}$ ) galaxies with high  $\lambda_{R_e}$  values implies that either our sample is biased against them (e.g. we only observed close to face-on massive galaxies) or these galaxies are rare. Since it is difficult to understand how such a bias could affect our sample, we need to conclude that indeed massive galaxies tend to have little or no baryonic angular momentum within one effective radius, and that the trend observed in Fig. 11 is real (see e.g. the upper panel with the histogram of  $M_{\text{vir}}$ ).

Interpreting the measured kinematic parameter  $\lambda_R$  as a proxy for the amount of stellar angular momentum per unit mass in the central region of early-type galaxies (see Appendix A), we can then discuss the origin of this angular momentum. The standard scenario for the formation of galaxy structures includes hierarchical clustering of cold dark matter haloes within which gas is cooling (Peebles 1969; Doroshkevich 1970; White 1984). The angular momentum of the dark matter haloes is thought to originate in cosmological torques and major mergers (e.g. Vitvitska et al. 2002), this hypothesis providing a reasonable frame for the formation of disc galaxies. If major mergers produce a significant increase in the specific angular momentum of the dark matter haloes at large radii (Vitvitska et al. 2002), minor mergers seem to just preserve or only slightly increase it with time (D’Onghia & Burkert 2004). But little is known about the expected distribution of the angular momentum of the *baryons* (van den Bosch et al. 2002; de Jong et al. 2004a), and even less if we focus on the central regions of galaxies (within a few effective radii). In fact, discs formed in numerical simulations are generally an order of magnitude too small (but see Dutton et al. 2007, for a possible solution).

Numerical simulations, whether they include a dissipative component or not, have helped us to understand how mergers influence the rotational support of the baryonic component in galaxies (see e.g. Barnes 1998; Somerville & Primack 1999; Cole et al. 2000; Bournaud, Jog & Combes 2005; Naab, Khochfar & Burkert 2006b). Stellar discs are cold and fragile systems, thus easily destroyed during major mergers which often lead to E-like remnants even in the presence of a moderate amount of gas (Naab, Jesseit & Burkert 2006a). Intermediate to minor mergers preserve part of the disc better, but in most cases a merger leads to a redistribution of the angular momentum of the central stellar component outwards (Bournaud, Combes & Jog 2004).

In this context, fast rotators have either preserved or regained their specific angular momentum in the central part. Since both very gas rich major and minor mergers seem to produce fast (disc-dominated) rotators (Cox et al. 2006; Robertson et al. 2006a), this requires either the absence of a major dry merger which would expel most of the angular momentum outwards or the rebuilding of a disc-like system via gas accretion. At high redshift ( $z > 2$ ), gas was abundant, and very gas rich mergers should have therefore been common. Robertson et al. (2006b) in fact claim that progenitors of early-type galaxies must be gas rich (gas fraction  $> 30$  per cent) to produce the tilt of the fundamental plane (FP). Dry major mergers are therefore expected to occur preferentially at lower  $z$ , with fast rotators not having suffered from such events. In the picture of the hierarchical formation of structures, minor mergers are more common than major mergers and we can thus expect galaxies (slow and fast rotators) to have suffered from more than one of these events up to  $z = 0$ .

The resulting specific angular momentum of fast rotators, as quantified by  $\lambda_R$ , is therefore expected to result mostly from a competition between (i) gas-rich minor mergers or other inflow of external gas that causes a gradual increase of  $\lambda_R$  (in the inner

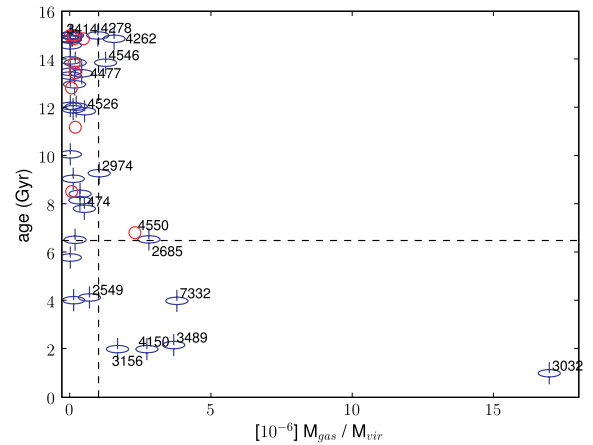


**Figure 12.** Average luminosity-weighted age of the stellar component versus the specific mass of ionized gas within the SAURON field of view  $M_{\text{gas}}/M_{\text{vir}}$  (ionized gas mass normalized by the virial mass; see Section 4.3). Symbols for fast and slow rotators are as in Fig. 5. Numbers for the ionized gas specific mass are derived from values in Papers IV and V, and average luminosity-weighted ages are from Kuntschner et al. (in preparation). The vertical and horizontal dashed lines show the limits of  $>10^{-6} M_{\text{gas}}/M_{\text{vir}}$  and 6.5 Gyr ( $z \sim 1$ ), respectively.

parts), and (ii) dissipationless dry minor mergers triggering disc instability and heating, and resulting in the transformation of disc material into a more spheroidal component, lowering  $\lambda_R$  (in the inner parts). The scenario described here follows the idea previously sketched by many authors (e.g. Bender et al. 1992; Kormendy & Bender 1996; Faber et al. 1997; Naab et al. 2006a) that dissipation is important in the formation process of fast rotating early-type galaxies. The ‘heating’ of the disc via star formation leads to an increase in the vertical dispersion, more isotropic and rounder galaxies, and therefore moving the galaxies along the anisotropy–ellipticity trend (Paper X) towards the slow rotators. A sudden removal of the gas (e.g. due to active galactic nucleus (AGN) feedback or ram-pressure stripping) might have ‘quenched’ this process, and quickly moved the galaxy from the ‘blue cloud’ to the ‘red sequence’ (Faber et al. 2005). Some galaxies may still have recently accreted some gas (e.g. via interaction with a companion; see Falcón-Barroso et al. 2004), and sometimes show the presence of a younger stellar population (such as NGC 3032, 3489, 4150, see Kuntschner et al. 2006, Paper VI, and also Paper VIII). In fact, all SAURON E/S0 galaxies which have luminosity-weighted ages of their stellar component lower than 6.5 Gyr ( $z \sim 1$ ) are fast rotators (Fig. 12; see also Kuntschner et al., in preparation). Among the 11 galaxies in our sample with a high ionized gas content ( $M_{\text{gas}}/M_{\text{vir}} > 10^{-6}$ ), only one is a slow rotator, namely the atypical disc galaxy NGC 4550. The slow rotator with the second highest gas content is the polar-ring galaxy NGC 3414 ( $M_{\text{gas}}/M_{\text{vir}} \sim 0.6 \times 10^{-6}$ ), NGC 4550 and NGC 3414 being in fact the two galaxies having deviant  $(a_4/a)_e$  values with respect to all other slow rotators (see Section 4.2).

Following the same line of argument, slow rotators need to have expelled most of their angular momentum within one effective radius outwards. This would require a significant fraction of the mass to be accreted during mergers with relatively gas-poor content. As emphasized above, all slow rotators with  $\lambda_{R_e} > 0.03$  (thus excluding the three slowest rotators which are consistent with zero rotation) have stellar kpc-size KDCs. Opposite to the smaller-scale KDCs in fast rotators (Section 4.4), the latter have a similar old



stellar population as the rest of the galaxy (Paper VIII), and thus were formed long ago when gas was more abundant than today. Indeed, numerical simulations of the formation of such structures seem to require the presence of some gas during the merger process followed by subsequent star formation, either in equal-mass mergers (Naab et al. 2006a) or in multiple intermediate or minor mergers (Bournaud, PhD thesis, Paris). Fig. 12 reveals that most slow rotators have a relatively modest fraction of ionized gas and are in fact older than  $\sim 6.5$  Gyr ( $z \sim 1$ ). The only two exceptions are, again, NGC 4550 which is very probably the result of the rare encounter of two disc galaxies with nearly exactly opposite spins (see Paper X), and NGC 3414 which shows the ‘rudiments of a disc’ (Sandage & Bedke 1994), and photometric structures reminiscent of polar-ring galaxies (van Driel et al. 2000) presumably formed via a tidal gas accretion event (Bournaud & Combes 2003). These results are consistent with the suggestion that slow rotators did not suffer from significant (in mass) recent dry mergers which may destroy or diffuse the large-scale KDCs. Minor mergers may still have recently occurred, and as above result in a competition of (slightly) lowering and increasing  $\lambda_R$ .

The three slowest rotators (NGC 4374, 4486 and 5846) may then correspond to the extreme end point of early-type galaxy evolution where dry mergers had a major role in the evolution, allowing  $\lambda_R$  to reach values consistent with zero in the central region. These galaxies are found in rather dense galactic environment and are expected to have experienced a significant number of mergers with galaxies which were themselves gas-depleted (due to ram-pressure stripping, efficient AGN feedback or earlier mergers), preferentially on radial orbits along the cosmological filaments (Boylan-Kolchin, Ma & Quataert 2006). As for the other slow rotators, the initial mergers will have been gas rich to place them on the FP, but later-on dry mergers are expected to be frequent as galaxies fall into the cluster potential well. The insignificant role of star formation in the late history of these galaxies is reflected in their both low specific gas content and old luminosity-weighted ages (Fig. 12). Overall, the trend we observe for early-type galaxies to have lower  $\lambda_R$  with increasing mass (Fig. 7) is consistent with the gradually more important role of (gas-poor) mergers when going from fast rotators to slow rotators.

Is this also consistent with the observed trend between  $\lambda_{R_c}$ ,  $M_{\text{vir}}$  and the cusp slope described above? Cores are thought to be the result of the scouring via a binary supermassive black hole (Faber et al. 1997; Merritt 2006, and references therein), the potential consequence of a merger. After a core is formed, a subsequent central accretion of gaseous material (from external or internal sources) followed by an episode of star formation could rejuvenate a cuspy luminosity profile, most probably in the form of an inner disc. If this scenario is correct, there should be a relation between the presence of a core and  $\lambda_{R_c}$ . The observation that massive slow rotators, thought to have significantly suffered from dissipationless mergers, all exhibit cores, and that small galaxies with high  $\lambda_{R_c}$  all contain cusps does indeed fit into this scenario. However, the fact that minor gas-free mergers may only remove part of the baryonic angular momentum and that gas can be accreted from, for example, external sources or stellar mass loss implies that there should not be a one-to-one relation, as indeed observed. Intriguingly, the two slow rotators with cusps (NGC 3414, 5813) both show the presence of a decoupled stellar disc-like component in their central a few hundreds of parsec (as witnessed by the amplitude of the associated  $h_3$  parameter; see Paper III). These may illustrate again the competition between gas-poor mergers and gas accreting processes in the making of galaxy structures.

## 6 CONCLUSIONS

Using two-dimensional stellar kinematics, we have argued that early-type galaxies can be divided into two broad dynamical classes. We have devised a new parameter  $\lambda_R$  to quantify the specific angular momentum in the stellar component of galaxies. This parameter, as applied within one effective radius to the 48 E and S0 galaxies of our SAURON sample, allowed us to disentangle the two classes of fast and slow rotators with a threshold value of 0.1. As emphasized in Section 3.2, fast and slow rotators exhibit qualitatively and quantitatively different stellar kinematics (see also Paper X). Galaxies with  $\lambda_R \leq 0.1$  form a distinct class characterized by little or no large-scale rotation, by the presence of KDCs and by significant KMs and/or velocity twists. This contrasts with galaxies for which  $\lambda_R > 0.1$ , which display global rotation along a well-defined apparent kinematic major axis that is nearly aligned with the photometric major axis. We have also shown that slow and fast rotators exhibit qualitatively different  $\lambda_R$  radial profiles and that slow rotators are unlikely to be face-on versions of fast rotators.

Besides the obvious difference in their angular momentum content, the main properties of the fast and slow rotators are as follows:

- (i) 75 per cent of the galaxies in our sample are fast rotators and 25 per cent are slow rotators. Most of the slow rotators are classified as Es, while fast rotators include a mix of Es and S0s.
- (ii) Within the slow rotators, three early-type galaxies have velocity fields consistent with near-zero rotation. These three objects (NGC 4374  $\equiv$  M 84, NGC 4486  $\equiv$  M 87 and NGC 5846) are bright and massive, nearly round galaxies.
- (iii) Fast rotators have ellipticities up to  $\epsilon \sim 0.6$ , in contrast to slow rotators which are relatively round systems with  $\epsilon < 0.3$ .
- (iv) Fast rotators tend to be relatively low-luminosity objects with  $M_B > -20.7$ . Slow rotators cover almost the full range of absolute magnitude of our sample, from faint discy galaxies such as NGC 4458 to bright slightly boxy galaxies such as NGC 5813, although they on average tend to be brighter than fast rotators. All slow rotators have Sérsic index  $n$  larger than 4, except the atypical galaxy NGC 4550.
- (v) More than 70 per cent of the galaxies in our sample exhibit multicomponent kinematic systems. As mentioned above, fast rotators have nearly aligned photometric and kinematic components, except for NGC 474 which exhibits obvious irregular shells. This contrasts with slow rotators which have significant KMs and/or velocity twists.
- (vi) All slow rotators, besides the three slowest rotators (for which stellar velocities are consistent with zero everywhere), exhibit a kpc-scale stellar KDC (see also Paper VIII).

These results are confirmed when including 18 additional galaxies observed with SAURON. Although our sample of 48 early-type galaxies is not a good representation of the galaxy luminosity distribution in the nearby Universe, it is the first to provide such a constraint for numerical simulations of galaxy formation and evolution. It is clear that a significantly larger and unbiased sample is required to probe the true distribution of  $\lambda_R$  in early-type galaxies and the fraction of slow and fast rotators. Even so, our sample should serve as a reference point for detailed numerical simulations of galactic systems in a cosmological context.

## ACKNOWLEDGMENTS

EE warmly thank Frank van den Bosch for insightful discussions. The SAURON project is made possible through grants

614.13.003, 781.74.203, 614.000.301 and 614.031.015 from NWO (Nederlandse Organisatie voor Wetenschappelijk Onderzoek) and financial contributions from the Institut National des Sciences de l'Univers, the Université Lyon I, the Universities of Durham, Leiden, and Oxford, the Programme National Galaxies, the British Council, PPARC grant 'Observational Astrophysics at Oxford 2002–2006' and support from Christ Church Oxford, and the Netherlands Research School for Astronomy NOVA. RLD is grateful for the award of a PPARC Senior Fellowship (PPA/Y/S/1999/00854) and postdoctoral support through PPARC grant PPA/G/S/2000/00729. The PPARC Visitors grant (PPA/V/S/2002/00553) to Oxford also supported this work. MC acknowledges support from a VENI award (639.041.203) by the Netherlands Organization for Scientific Research (NWO) and a PPARC Advanced Fellowship (PP/D005574/1). GVDV acknowledges support provided by NASA through grant NNG04GL47G and through Hubble Fellowship grant HST-HF-01202.01-A awarded by the Space Telescope Science Institute, which is operated by the Association of Universities for Research in Astronomy, Inc., for NASA, under contract NAS 5-26555. JFB acknowledges support from the Euro3D Research Training Network, funded by the EC under contract HPRN-CT-2002-00305. This paper is based on observations obtained at the William Herschel Telescope, operated by the Isaac Newton Group in the Spanish Observatorio del Roque de los Muchachos of the Instituto de Astrofísica de Canarias. This project made use of the HyperLeda (<http://leda.univ-lyon1.fr>) and NED data bases. Part of this work is based on data obtained from the ESO/ST-ECF Science Archive Facility. Photometric data were obtained (in part) using the 1.3-m McGraw-Hill Telescope of the MDM Observatory.

## REFERENCES

- Bacon R. et al., 1995, *A&AS*, 113, 347  
 Bacon R. et al., 2001, *MNRAS*, 326, 23 (Paper I)  
 Barnes J. E., 1998, in Kennicutt R. C., Jr, Schweizer F., Barnes J. E., Friedli D., Martinet L., Pfenniger D., eds, *Saas-Fee Advanced Course 26: Galaxies: Interactions and Induced Star Formation Dynamics of Galaxy Interactions*. Springer-Verlag, Berlin, p. 275  
 Bender R., 1988, *A&A*, 202, L5  
 Bender R., Moellenhoff C., 1987, *A&A*, 177, 71  
 Bender R., Doebereiner S., Moellenhoff C., 1988, *A&AS*, 74, 385  
 Bender R., Burstein D., Faber S. M., 1992, *ApJ*, 399, 462  
 Bender R., Saglia R. P., Gerhard O. E., 1994, *MNRAS*, 269, 785  
 Binney J., 1978, *MNRAS*, 183, 501  
 Binney J., 2005, *MNRAS*, 363, 937  
 Bournaud F., Combes F., 2003, *A&A*, 401, 817  
 Bournaud F., Combes F., Jog C. J., 2004, *A&A*, 418, L27  
 Bournaud F., Jog C. J., Combes F., 2005, *A&A*, 437, 69  
 Boylan-Kolchin M., Ma C.-P., Quataert E., 2006, *MNRAS*, 369, 1081  
 Burkert A., Naab T., 2005, *MNRAS*, 363, 597  
 Caon N., Capaccioli M., D'Onofrio M., 1993, *MNRAS*, 265, 1013  
 Cappellari M., Copin Y., 2003, *MNRAS*, 342, 345  
 Cappellari M., Emsellem E., 2004, *PASP*, 116, 138  
 Cappellari M. et al., 2006, *MNRAS*, 366, 1126 (Paper IV)  
 Cappellari M. et al., 2007, *MNRAS*, in press (doi:10.1111/j.1365-2966.2007.11963.x) (Paper X, this issue)  
 Cole S., Lacey C. G., Baugh C. M., Frenk C. S., 2000, *MNRAS*, 319, 168  
 Cox T. J., Dutta S. N., Di Matteo T., Hernquist L., Hopkins P. F., Robertson B., Springel V., 2006, *ApJ*, 650, 791  
 Davies R. L., Efstathiou G., Fall S. M., Illingworth G., Schechter P. L., 1983, *ApJ*, 266, 41  
 de Jong R. S., Kassin S., Bell E. F., Courteau S., 2004a, in Ryder S., Pisano D., Walker M., Freeman K., eds, *Proc. IAU Symp. 220, Properties of Dark Matter Haloes in Disk Galaxies*. Astron. Soc. Pac., San Francisco, p. 281  
 de Jong R. S., Simard L., Davies R. L., Saglia R. P., Burstein D., Colless M., McMahan R., Wegner G., 2004b, *MNRAS*, 355, 1155  
 de Vaucouleurs G., de Vaucouleurs A., Corwin H. G., Jr, Buta R. J., Paturel G., Fouque P., 1991, *Third Reference Catalogue of Bright Galaxies*. Springer-Verlag, Berlin, p. 7  
 de Zeeuw P. T. et al., 2002, *MNRAS*, 329, 513 (Paper II)  
 D'Onghia E., Burkert A., 2004, *ApJ*, 612, L13  
 Doroshkevich A. G., 1970, *Astrophysics*, 6, 320  
 Dutton A. A., van den Bosch F. C., Dekel A., Courteau S., 2007, *ApJ*, 654, 27  
 Emsellem E. et al., 2004, *MNRAS*, 352, 721 (Paper III)  
 Faber S. M. et al., 1997, *AJ*, 114, 1771  
 Faber S. M. et al., 2005, *ApJ*, submitted (astro-ph/0506044)  
 Falcón-Barroso J. et al., 2004, *MNRAS*, 350, 35  
 Ferrarese L. et al., 2006, *ApJS*, 164, 334  
 Fisher D., 1997, *AJ*, 113, 950  
 Franx M., 1988, *Structure and Kinematics of Elliptical Galaxies*. Rijksuniversiteit, Leiden  
 Franx M., Illingworth G., Heckman T., 1989, *AJ*, 98, 538  
 Fritze v. Alvensleben U., 2004, in Block D. L., Puerari I., Freeman K. C., Groess R., Block E. K., eds, *Astrophys. Space Sci. Library Vol. 319, Penetrating Bars Through Masks of Cosmic Dust*. Kluwer, Dordrecht, p. 81  
 Graham A. W., Guzmán R., 2003, *AJ*, 125, 2936  
 Hao C. N., Mao S., Deng Z. G., Xia X. Y., Wu H., 2006, *MNRAS*, 370, 1339  
 Hubble E. P., 1936, *Realm of the Nebulae*. Yale Univ. Press, New Haven  
 Illingworth G., 1977, *ApJ*, 218, L43  
 Jaffe W., 1983, *MNRAS*, 202, 995  
 Jedrzejewski R. I., 1987, *MNRAS*, 226, 747  
 Jorgensen I., Franx M., 1994, *ApJ*, 433, 553  
 Kissler-Patig M., Gebhardt K., 1998, *AJ*, 116, 2237  
 Kormendy J., Bender R., 1996, *ApJ*, 464, L119 (KB96)  
 Krajnović D., Cappellari M., de Zeeuw P. T., Copin Y., 2006, *MNRAS*, 366, 787  
 Kuntschner H. et al., 2006, *MNRAS*, 369, 497  
 Lauer T. R., 1985, *MNRAS*, 216, 429  
 Lauer T. R. et al., 2005, *AJ*, 129, 2138  
 McDermid R. M. et al., 2006, *MNRAS*, 373, 906 (Paper VIII)  
 Mei S. et al., 2005, *ApJ*, 625, 121  
 Merritt D., 2006, *ApJ*, 648, 976  
 Michard R., 1994, *A&A*, 288, 401  
 Naab T., Jesseit R., Burkert A., 2006a, *MNRAS*, 372, 839  
 Naab T., Khochfar S., Burkert A., 2006b, *ApJ*, 636, L81  
 Paturel G., Petit C., Prugniel P., Theureau G., Rousseau J., Brouty M., Dubois P., Cambrésy L., 2003, *A&A*, 412, 45  
 Peebles P. J. E., 1969, *ApJ*, 155, 393  
 Ravindranath S., Ho L. C., Peng C. Y., Filippenko A. V., Sargent W. L. W., 2001, *AJ*, 122, 653  
 Rest A., van den Bosch F. C., Jaffe W., Tran H., Tsvetanov Z., Ford H. C., Davies J., Schafer J., 2001, *AJ*, 121, 2431  
 Rix H.-W., White S. D. M., 1990, *ApJ*, 362, 52  
 Rix H.-W., Franx M., Fisher D., Illingworth G., 1992, *ApJ*, 400, L5  
 Robertson B., Bullock J. S., Cox T. J., Di Matteo T., Hernquist L., Springel V., Yoshida N., 2006a, *ApJ*, 645, 986  
 Robertson B., Cox T. J., Hernquist L., Franx M., Hopkins P. F., Martini P., Springel V., 2006b, *ApJ*, 641, 21  
 Rubin V. C., Graham J. A., Kenney J. D. P., 1992, *ApJ*, 394, L9  
 Ryden B. S., Terndrup D. M., Pogge R. W., Lauer T. R., 1999, *ApJ*, 517, 650  
 Sandage A., 2004, in Block D. L., Puerari I., Freeman K. C., Groess R., Block E. K., eds, *Astrophys. Space Sci. Library Vol. 319, Penetrating Bars Through Masks of Cosmic Dust Episodes*. Kluwer, Dordrecht, p. 39  
 Sandage A., Bedke J., 1994, *The Carnegie Atlas of Galaxies*. Carnegie Institution of Washington with The Flintridge Foundation, Washington DC

- Sarzi M. et al., 2006, MNRAS, 366, 1151 (Paper V)  
 Sembach K. R., Tonry J. L., 1996, AJ, 112, 797  
 Somerville R. S., Primack J. R., 1999, MNRAS, 310, 1087  
 Spitzer L. J., Baade W., 1951, ApJ, 113, 413  
 Statler T. S., 2001, AJ, 121, 244  
 Tonry J. L., Dressler A., Blakeslee J. P., Ajhar E. A., Fletcher A. B., Luppino G. A., Metzger M. R., Moore C. B., 2001, ApJ, 546, 681  
 Trujillo I., Erwin P., Asensio Ramos A., Graham A. W., 2004, AJ, 127, 1917  
 Tully R. B., 1988, *Nearby Galaxies Catalog*. Cambridge Univ. Press, Cambridge, p. 221  
 Turnbull A. J., Bridges T. J., Carter D., 1999, MNRAS, 307, 967  
 van den Bergh S., 1990, ApJ, 348, 57  
 van den Bosch F. C., Abel T., Croft R. A. C., Hernquist L., White S. D. M., 2002, ApJ, 576, 21  
 van der Marel R. P., Franx M., 1993, ApJ, 407, 525  
 van Driel W., Arnaboldi M., Combes F., Sparke L. S., 2000, A&AS, 141, 385  
 Vitvitska M., Klypin A. A., Kravtsov A. V., Wechsler R. H., Primack J. R., Bullock J. S., 2002, ApJ, 581, 799  
 Wernli F., Emsellem E., Copin Y., 2002, A&A, 396, 73  
 White S. D. M., 1984, ApJ, 286, 38  
 Young L. M., 2005, ApJ, 634, 258

## APPENDIX A: THE ANGULAR MOMENTUM OF GALAXIES AND $\lambda_R$

The criterion we wish to define should clearly separate the slow and fast rotators. The first guess is to take something equivalent to the total angular momentum, which should be expressed as something like  $\langle X|V| \rangle$  where  $X$  is the distance to the spin axis. To avoid having to determine that axis, we chose  $\langle R|V| \rangle$ , where  $R$  is the distance to the centre. The absolute value of  $V$  is used as we are interested in the presence of local streaming motion (e.g. see NGC 4550). This is then naturally normalized by  $\langle X\sqrt{V^2 + \sigma^2} \rangle$  where  $V^2 + \sigma^2$  is the second-order velocity moment.

Another route would be to get closer to some physical quantity such as the angular momentum per unit mass. This can be represented via the spin parameter (e.g. Peebles 1969)

$$\lambda = \frac{J\sqrt{|E|}}{GM^{2.5}}, \quad (\text{A1})$$

where  $J, E$  and  $M$  are the total angular momentum, energy and mass, and  $G$  is Newton's constant of gravity. The derivation of  $\lambda$  in principle requires an accurate distance for each galaxy. Since we wish to stay close to our SAURON measurements, we need to define something which can be readily evaluated. This is possible by first rewriting  $\lambda$  as

$$\lambda = \frac{J/M\sqrt{|E|/M}}{GM}. \quad (\text{A2})$$

For two-dimensional integral-field data, we can approximate the spin parameter by using the scalar virial relations and sky averaging over the field-of-view, weighted with the surface brightness. The scalar virial relations are  $2E = -2K = W$ , with the total kinetic and potential energy related to the mean-square speed of the system's stars  $V_{\text{rms}}$ , respectively, as  $2K/M = V_{\text{RMS}}^2$  and  $W/M = -GM/r_g$ . Here,  $r_g$  is the gravitational radius, which can be related to the half-mass radius  $r_h$  given the mass model of the stellar system. For a spherical symmetric Jaffe (1983) model, we have  $r_g = 2r_h$ .

When relating  $r_g$  (or  $r_h$ ) to the observed effective radius  $R_e$ , we have to take into account the projection as a function of the viewing angle of the stellar system which in general is not spherical. Furthermore, while  $r_g$  and  $r_h$  are related to the mass distribution,  $R_e$  depends on the light distribution. Therefore, given  $r_g = \kappa_R R_e$

the conversion factor  $\kappa_R$  is a function of the mass model, viewing direction and mass-to-light ratio. In a similar way, a conversion factor is needed in the approximation of the total angular momentum by the observed radius times velocity:  $J/M = \kappa_J R|V|$  (see Franx 1988). Furthermore, while  $V_{\text{RMS}}^2$  is the *total* mean-square speed, we only observe velocity moments projected along the line-of-sight, e.g.  $V$  and  $\sigma$ . In order to retrieve  $V_{\text{RMS}}^2$ , we should therefore allow multiplying factors  $\kappa_V$  and  $\kappa_S$  associated with the corresponding observed  $V^2$  and  $\sigma^2$  (in the case of an isothermal sphere,  $\kappa_V = 1$  and  $\kappa_S = 3$ ).

We thus find the following expressions:

$$J/M = \kappa_J \langle R|V| \rangle, \quad (\text{A3})$$

$$2E/M = - \langle \kappa_V V^2 + \kappa_S \sigma^2 \rangle, \quad (\text{A4})$$

$$GM = \kappa_R \langle R (\kappa_V V^2 + \kappa_S \sigma^2) \rangle, \quad (\text{A5})$$

resulting in an approximate spin parameter

$$\lambda \sim \frac{\kappa_J}{\kappa_R \sqrt{2}} \frac{\langle R|V| \rangle \sqrt{\langle \kappa_V V^2 + \kappa_S \sigma^2 \rangle}}{\langle R (\kappa_V V^2 + \kappa_S \sigma^2) \rangle}. \quad (\text{A6})$$

For simplicity, we will use the observed second-order velocity moment  $V^2 + \sigma^2$ , so that both  $\kappa_V = 1$  and  $\kappa_S = 1$ , and thus define  $\lambda_f$  as

$$\lambda_f \equiv \frac{\langle R|V| \rangle \sqrt{\langle V^2 + \sigma^2 \rangle}}{\langle R(V^2 + \sigma^2) \rangle}. \quad (\text{A7})$$

We finally approximate  $\lambda_f$  with  $\lambda_R$  by writing

$$\lambda_f \sim \lambda_R \equiv \frac{\langle R|V| \rangle}{\langle R\sqrt{V^2 + \sigma^2} \rangle}. \quad (\text{A8})$$

When deriving the values of both  $\lambda_f$  and  $\lambda_R$  for the 48 E and S0 SAURON galaxies, we indeed find a tight relation:

$$\lambda_R = (0.95 \pm 0.04) \times \lambda_f. \quad (\text{A9})$$

This relation is in fact also valid for the two-integral models as derived in Appendix B, so that we expect  $\lambda_R$  to be roughly equal to (though slightly smaller than)  $\lambda_f$ . For typical values of the conversion factors,  $\kappa_J = 2$ ,  $\kappa_R = 3$ , we therefore find that  $\lambda \sim \sqrt{2}/3 \lambda_R$ .

An alternative to  $\lambda_R$  is the unbounded  $\lambda'_R = \langle R|V| \rangle / \langle R\sigma \rangle$ . In the context of early-type galaxies, we favour  $\lambda_R$  which includes a mass-like normalization by the second-order velocity moment  $V^2 + \sigma^2$ . For isotropic (two-integral) models, this implies  $\lambda_R \sim \sqrt{\epsilon}$ . For slow rotators  $\lambda_R \sim \lambda'_R$ , since these galaxies have by definition small mean stellar velocities.

## APPENDIX B: TWO-INTEGRAL MODELS

In order to examine the behaviour of  $\lambda_R$  in more detail, we constructed two-integral dynamical Jeans models for seven SAURON galaxies using the MGE formalism, namely NGC 524, 3377, 4459, 4486, 4552, 4621 and 5813. Details on the assumptions and resulting mass models for these galaxies can be found in Paper IV. For each galaxy, we assumed eight different inclinations ( $5^\circ$ ,  $15^\circ$ ,  $25^\circ$ ,  $35^\circ$ ,  $50^\circ$ ,  $65^\circ$ ,  $80^\circ$  and  $90^\circ$ , the latter corresponding to an edge-on view), and derived the first two line-of-sight velocity moments up to  $1R_e$ .

These models were used to obtain measurements of  $\lambda_R$ ,  $\lambda_f$  and  $V/\sigma$  to determine whether these three quantities behave similarly with respect to basic parameters such as the inclination or anisotropy parameter. We first obtain that  $\lambda_R = (0.93 \pm 0.04) \times \lambda_f$ , a correlation very similar to what was found for the observed 48 SAURON

galaxies (see Appendix A). The variation of  $\lambda_R$  with inclination follows that of  $V/\sigma$  within better than 10 per cent for two-integral models. These results do not depend on the global anisotropy, as long as the internal dynamics of the model are fixed before changing the viewing angle. A radial variation in the anisotropy profile can, however, significantly change this situation, as  $\lambda_R$  includes an additional explicit dependence on radius. Assuming isotropy for all seven MGE Jeans models, we observe a tight correlation between  $\lambda_R$  and  $V/\sigma$ . A simple approximation for the relation between  $\lambda_R$  and  $V/\sigma$  can then be obtained by introducing a scaling factor  $\kappa$ :

$$\lambda_R = \frac{\langle RV \rangle}{\langle R \sqrt{V^2 + \sigma^2} \rangle} \approx \frac{\kappa (V/\sigma)}{\sqrt{1 + \kappa^2 (V/\sigma)^2}}. \quad (\text{B1})$$

Using our two-integral models, we find a best-fitting relation with  $\kappa = 1.2 \pm 0.1$ , slightly higher than but still consistent with the best-fitting value  $\kappa = 1.1 \pm 0.1$  obtained using our 48 SAURON Es and S0s. We can in fact directly solve for  $\kappa$  in equation (B1) in terms of the values of  $\lambda_R$  and  $V/\sigma$  measured for individual two-integral models: there is in fact a rather large spread in the values of  $\kappa$ , which ranges from 1 and 1.4, depending on the galaxy. This shows that non-homology is an important driver of changes in  $\lambda_R$  at constant  $V/\sigma$ .

Another important issue when deriving  $\lambda_R$  and  $V/\sigma$  comes from the presence of noise in the measurements. When  $V$  is sufficiently large, the random errors in the kinematic measurements will affect both  $\lambda_R$  and  $V/\sigma$  randomly. As  $V$  becomes small in absolute value,  $\langle V^2 \rangle$  and  $\langle R|V| \rangle$  become increasingly biased (being artificially increased), which affects estimates of  $\lambda_R$  and  $V/\sigma$ . In Fig. B1, we show the effect of a random error of  $10 \text{ km s}^{-1}$  in both  $V$  and  $\sigma$  (typical in the outer part of SAURON kinematic maps; see Paper III) on both  $\lambda_R$  and  $V/\sigma$ , in terms of  $\lambda_R$ .  $\Delta$  is the difference between the measured value (with noise) and the expected one (noiseless) and is plotted with respect to the true  $\lambda_R$  value. The effect is in general

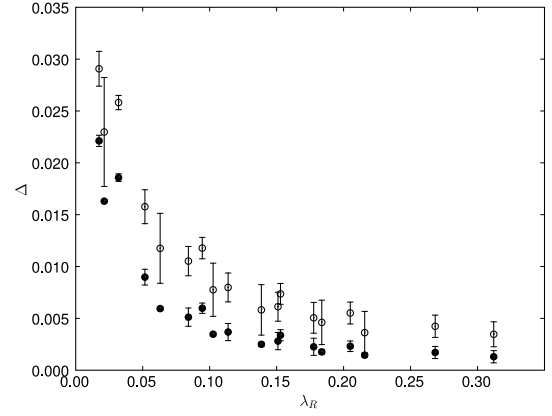


**Figure B1.** Effect of noise in the kinematics on the estimate of  $\lambda_R$  (filled symbols) and  $V/\sigma$  (empty symbols).  $\Delta$ , the difference between the measured value (with noise) and the expected one (noiseless), is plotted against  $\lambda_R$ . The input noise has been set to  $10 \text{ km s}^{-1}$  for both  $V$  and  $\sigma$ .

relatively small, of the order of 7 per cent on  $\lambda_R$  and almost 15 per cent on  $V/\sigma$ , for  $\lambda_R \sim 0.1$ . When  $V$  is close to zero everywhere, as is the case for the three SAURON galaxies with the lowest  $\lambda_R$  values, the presence of noise yields an overestimate of about 0.02 in  $\lambda_R$  (depending on the velocity dispersion values), an effect consistent with the observed values for these galaxies (see Fig. 5). As expected, Fig. B1 also shows that  $\lambda_R$  is in general about a factor of 2 less sensitive to errors in the kinematic measurements than  $V/\sigma$ .

This paper has been typeset from a  $\text{\LaTeX}$  file prepared by the author.